2010

Sensing and Control of MEMS Accelerometers Using Kalman Filter

Kai Zhang
Cleveland State University

SENSING AND CONTROL OF MEMS ACCELEROMETERS USING KALMAN FILTER

KAI ZHANG

Bachelor Degree of Science of Electronics in Radio-Communication

East China Normal University, China

June, 2000

submitted in partial fulfillment of requirements for the degree

MASTER OF SCIENCE IN ELECTRICAL ENGINEERING

at the

CLEVELAND STATE UNIVERSITY

December, 2010

This thesis has been approved
for the Department of Electrical and Computer Engineering
and the College of Graduate Studies by

_____

Thesis Committee Chairperson, Lili Dong

_____

Department/Date

_____

Thesis Committee Member, Charles Alexander

_____

Department/Date

_____

Thesis Committee Member, Siu-Tung Yau

_____

Department/Date

To

my beloved parents Guoxiang Zhang and Huijin Jin

and

my wife Yi Liu

ACKNOWLEDGEMENTS

I would like to express my sincere gratitude to my advisor Dr. Lili Dong, for her ingenious commitment, encouragement and highly valuable advices she provided me over the entire graduate study in Cleveland State University. Her rigorous attitudes to do the research and helpful suggestions to solve problems will affect me during my whole professional career.

I would also like to thank my committee members Dr. Charles Alexander and Dr. Siu-Tung Yau for their support and advice.

I thank my classmates Yao Zhang, Silu You and Honglei Zhang for their encouragement and intellectual input during entire course of this thesis.

My thanks also go to my parents and parents-in-law, who always encourage me all the time. Also thanks to my brothers, Ji Lin and Weidong Cai who support me during my hard time.

Last but not least, I would like to thank my wife Yi Liu, my son Kenny Zhang, and my daughter Kitty Zhang for their consistent love, support, understanding, and encouragement and for the whole life we experienced and expect together.

SENSING AND CONTROL OF MEMS ACCELEROMETERS USING KALMAN FILTER

KAI ZHANG

ABSTRACT

Surface micromachined low-capacitance MEMS capacitive accelerometers which integrated CMOS readout circuit generally have a noise above 0.02*g*. Force-to-rebalance feedback control that is commonly used in MEMS accelerometers can improve the performances of accelerometers such as increasing their stability, bandwidth and dynamic range. However, the controller also increases the noise floor. There are two major sources of the noise in MEMS accelerometer. They are electronic noise from the CMOS readout circuit and thermal-mechanical Brownian noise caused by damping. Kalman filter is an effective solution to the problem of reducing the effects of the noises through estimating and canceling the states contaminated by noise. The design and implementation of a Kalman filter for a MEMS capacitive accelerometer is presented in the thesis in order to filter out the noise mentioned above while keeping its good performance under feedback control. The dynamic modeling of the MEMS accelerometer system and the controller design based on the model are elaborated in the thesis. Simulation results show the Kalman filter gives an excellent noise reduction, increases the dynamic range of the accelerometer, and reduces the displacement of the mass under a closed-loop structure.

TABLE OF CONTENTS

NOMENCLATURE

MEMS:	Micro-Electro-Mechanical System
SNR:	Signal to noise ratio
DR:	Dynamic range
AD:	Analog to Digital
DSP:	Digital signal process
RIE:	Reactive ion etch
SEM:	Scanning electron micrographs
PI:	Proportional-integral
PSD:	Power spectral density
EKF:	Extended Kalman filter
LTI:	Linear time invariant
STD:	Standard deviation

LIST OF FIGURES

LIST OF TABLES

Table **Page**

CHAPTER I

INTRODUCTION

This chapter will give a brief review of the existing MEMS accelerometers and the sensing and control methods used in accelerometers. In addition, the proposed control solution to be employed in this thesis will be discussed.

1.1 Introduction

With the development of micro fabrication technology, Micro-Electro-Mechanical System (MEMS) which integrated mechanical sensors and actuators with electrical circuits has been broadly applied to various fields such as airbags in automotives, bio-medical area, and military system. This thesis will focus on MEMS capacitive accelerometer which has two fundamental problems: sensing and control.

MEMS technology gives possibility to integrate complex systems into a small single chip with low cost and multiple functions. However, the miniaturized devices also reduce the signal to noise ratio (SNR) and the dynamic range (DR), and also increase the system uncertainties during the manufacturing process.

Inertial MEMS sensors including MEMS accelerometers and gyroscopes occupy more than 20% of MEMS markets. MEMS accelerometers alone have the second largest sales volume after pressure sensors. As an acceleration and deceleration sensor, MEMS accelerometers have been extensively applied to airbag deployment systems in automobiles [1].

Fig 1 shows the performance and cost of different MEMS fabrication technologies which can be used to manufacture MEMS accelerometers. Capacitive sensing mechanism structure is the most popular in MEMS accelerometer.

.

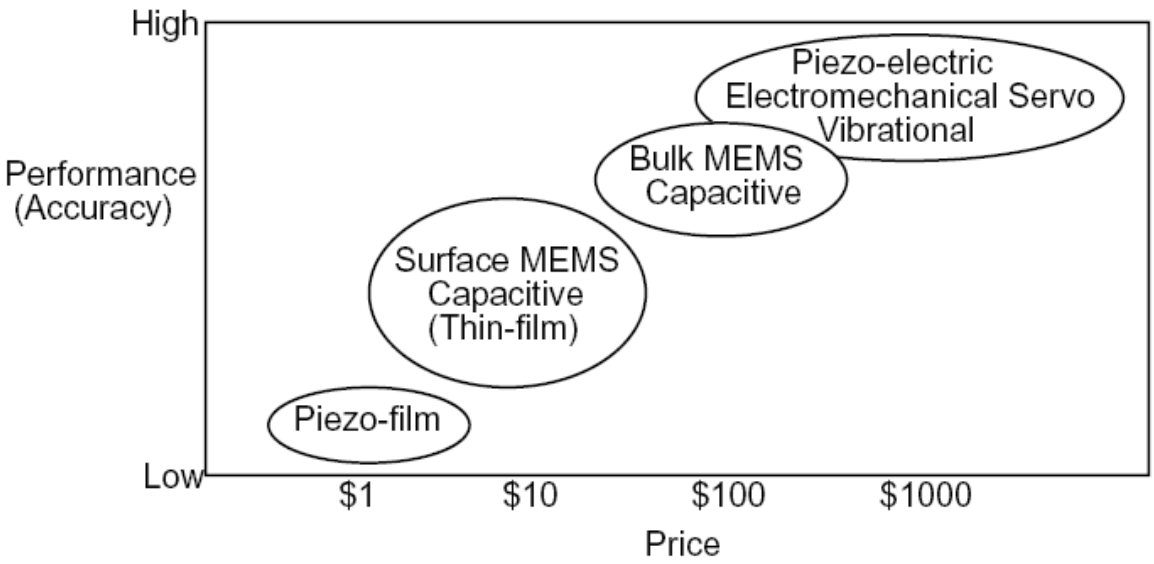

Figure 1: Performance and cost of different MEMS accelerometer [1]

As shown in Fig 1, bulk and surface micromachining technologies are two particular methods used in fabricating capacitive sensing accelerometers. Compared to surface micro-machined accelerometers, the bulk micromachined devices have high sensitivity and low noise floor since they have large mass and more sensing capacitors. However, the surface

micromachined devices are low cost and easy to be integrated with signal processing circuits [2] while low cost and easy implementation are always two desirable features in MEMS. Moreover, capacitive sensing mechanism is currently the most popular sensing technology in MEMS accelerometer. Compared to other two sensing mechanisms which are piezoresistive sensing and tunnel current sensing, capacitive sensing has the advantages of low power dissipation, low cost, and low temperature coefficients [1]. Therefore, in this thesis, we will construct Kalman filter observer based on surface micro-machined capacitive accelerometers.

Brownian noise caused by damping effect and electronic noise from CMOS readout circuit are two major noise sources in both bulk and surface micromachined capacitive accelerometers. Brownian noise is higher in surface micromachined accelerometers than in bulk micromachined ones because of the small mass of a surface micro-machined accelerometer. Noise floor is the measurement of the signal created by noise sources and unwanted signals. We can not detect a signal if its value is under noise floor. The value of noise floor normally changes with different frequency and has a unit relates to frequency. The Brownian noise in surfaced micro-machined accelerometers has the noise floor between $10-100\mu g/rtHz$. The noise floor of electronic noise in the surface micromachined accelerometer is above $20\mu g/rtHz$ and is much more critical than the one in the bulk micromachined accelerometers because of the lower capacitance in surface micro-machined accelerometers.

Besides noise, the sensing accuracy of low-cost surface micro-machined accelerometer is also limited by the nonlinearities and system uncertainties due to fabrication imperfections. Therefore, a feedback controller is essential for surface micro-machined accelerometers to compensate for the fabrication imperfections and improve its performance. It can reduce the

offsets caused by mechanical imperfections and increase the bandwidth, sensitivity and dynamic range of accelerometers. Nevertheless, noise is still a challenging problem to the surface micro-machined accelerometers even with a feedback controller. This leads us to use Kalman filter to reduce the noise. The Kalman filter will be functioning as an observer in feedback control.

1.2 Existing sensing and control solutions for MEMS accelerometers

Three major capacitive sensing accelerometer circuit designs for accelerometers are reported in current literature. They are modulation/demodulation voltage sensing [2, 3, 4], current sensing [5] and switch capacitor charge sensing [6]. The most popular method is switch capacitor read-out circuit sensing, which is also the sensing method used in this thesis. The modulation/demodulation voltage sensing is more accurate than the switch capacitor charge sensing, but it requires more electronic components such as buffer, amplifier, and high speed sampling switch. The modulation/demodulation voltage sensing is expensive and makes the fabrication process complicated. The current sensing is noisy as mentioned in [5].

In addition, two major control methods are applied in capacitive accelerometers. They are force-to-rebalance closed-loop control [4, 7] and a compensator in $\Delta\Sigma$ loop control [8, 9, 10, 11]. Currently, most MEMS products use open-loop control method instead of closed-loop control due to their space limit and their low requirements for dynamic range. The complication and high cost of closed-loop operation also limit its use. However, compared to open-loop control method, closed-loop control is more robust against noise and external disturbances. Force-to-rebalance closed-loop control has been applied in Analog Devices'

recent ADXL series MEMS accelerometers. A readout circuit and a $\Delta\Sigma$ loop with feed-back compensator have been introduced in [8], [9], [10] and [11]. The $\Delta\Sigma$ modulators are also called over-sampling Analog to Digital (AD) converters. A digital signal has higher noise immunity than that of analog signal. In addition, the digital signal can be easily implemented using powerful digital signal process (DSP) algorithm.

The bulk micro-machined accelerometer in [8] gives a lower noise floor at $3.7\mu g/rtHz$, because it has a big mass of $10^{-6}kg$ and large capacitance at μF level and also uses $\Delta\Sigma$ compensator control. In [12], bulk micro-machining technology shows a more significant noise floor at $2200\mu g/rtHz$ due to nonlinearities and uncertain parameter effects through open-loop control method. The capacitive accelerometer in [9] shows more noise at $1600\mu g/rtHz$ since it uses surface micro-machined process with smaller mass at $10^{-9}kg$ and capacitance at pF. All of the accelerometers in [3], [4], [10] and [11] are surface micro-machined accelerometers with modulation voltage sensing. But they use different control methods including open-loop control [3], force-to-rebalance control [4] and $\Delta\Sigma$ compensator [10] [11]. In [11], an advanced sensing method named chopper stabilized voltage modulation is used and makes the noise floor at $4.6\mu g/rtHz$. Force-to-rebalance control method in [4] gives a $500\mu g/rtHz$ noise floor which is larger than open-loop control in [3] at $200\mu g/rtHz$ because of controller post-set which is going to discuss in chapter 3. From above the literature review, we can see the more complicated and advanced sensing and control methods we use, the smaller noise floor we will obtain.

Although different fabrication methods (such as surface and bulk micro-machining fabrications) could affect the performances of MEMS accelerometers in noise rejection and sensitivity, appropriate sensing and control strategy could compensate for the mechanical

imperfections and improve the performance of accelerometers. The growing applications of control designs have been investigated and used to overcome the noise problems caused by low cost surface micromachined fabrication. In this thesis, we will discuss a surface micro-machined MEMS capacitive accelerometer with switch capacitive sensing and force-to-rebalance control strategy.

1.3 Proposed control solution in this thesis

Our goal is to reduce the noise in a low-cost surface-micro-machined MEMS accelerometer while keeping its good sensing performance through a close-loop control system. Our method is to use the Kalman filter as an observer to estimate the states of accelerometer using measured outputs, and then instead of feeding back the noised output signal to the input of the MEMS accelerometer system, we use the estimated states which have much lower noise influence to close the system. This method not only gives a noiseless estimated output, but also improves the control performance with noiseless feedback signal. Using this type of technique (i.e. Kalman filter), we can improve the performance of low-cost surface-machined MEMS accelerometer and replace the costly bulk micromachined accelerometer with it. The Kalman filter can be added in a microcontroller or DSP chips which have already been used in MEMS accelerometer application.

1.4 Organization

The organization of this thesis is as follows. Chapter 2 presents the surface micromachining MEMS capacitive accelerometer which we are going to construct the

Kalman filter on. This chapter is going to give description of fabrication process, to establish the dynamic modeling, and to conduct frequency-domain analyses. In Chapter 3, a noise consideration will be discussed. Electronic noise from the CMOS readout circuit and thermal-mechanical Brownian noise caused by damping are reviewed and analyzed. Chapter 4 presents the design of Kalman filter and its advantages and disadvantages. Chapter 5 simulates Kalman filter on a capacitive accelerometer. It also compares the simulation results of the Kalman filter with the ones of other existing solutions. Chapter 6 makes the concluding remarks and suggests future research directions.

CHAPTER II

MEMS CAPACITIVE ACCELEROMETER

In this chapter, the modeling of a typical MEMS accelerometer, including sensing principle and electronic readout circuit will be introduced. In addition, the open-loop and closed-loop MEMS accelerometers are discussed. Based upon the modeling of accelerometers, stability, measurement performance and frequency response will be investigated.

2.1 Surface micromachining process and structure

The process flow of surface micro-machining technology with CMOS circuit fabrication is illustrated in Fig 2 [3]. This technology was initially developed by Carnegie Mellon University. As shown in Fig. 2, there are two steps after the standard CMOS fabrication process. An anisotropic reactive ion etch (RIE) with CHF_3/O_2 is the first step to etch away the silicon oxide which is not covered by the metal layer. Then an isotropic RIE with SF_6/O_2 is used to remove the underlying silicon layer and release the microstructure.

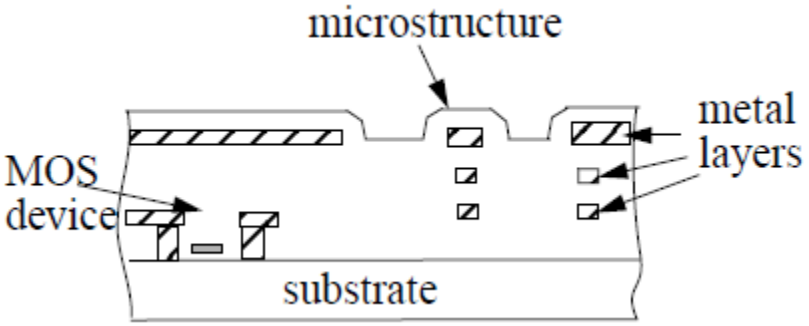

(a) After CMOS fabrication

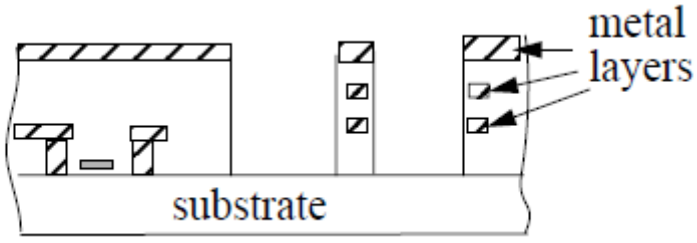

(b) After anisotropic RIE

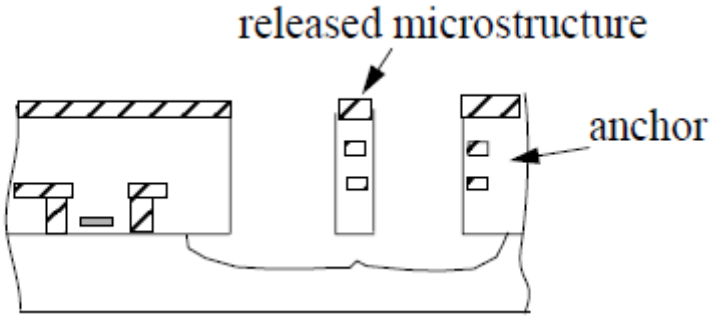

(c) After isotropic RIE

Figure 2: CMOS-MEMS process flow [3]

The two dry etching steps make the CMOS-MEMS micromachining not expensive to archive. And the integration of mechanical structure and electronics gives more possibility to implement sensing and control methods. But thin-film structure limits the device's performance. Small mass not only causes the low sensitivity to the acceleration at the range

of1 mv/g, but increases the Brown noise. Moreover low capacitance of CMOS circuit also causes a large electronics noise.

A prototype of CMOS-MEMS accelerometer is shown in Fig 3. The seismic mass with parallel capacitor fingers is connected to the substrate by springs. The acceleration on the substrate makes the seismic mass up and down, and consequently changes the capacitance between each two fingers. The change of capacitance will be converted into electrical signal such as voltage. Each two paralleled capacitor fingers also form an electrostatic actuator that can be used to create electrostatic forces for force-to-rebalanced feedback control.

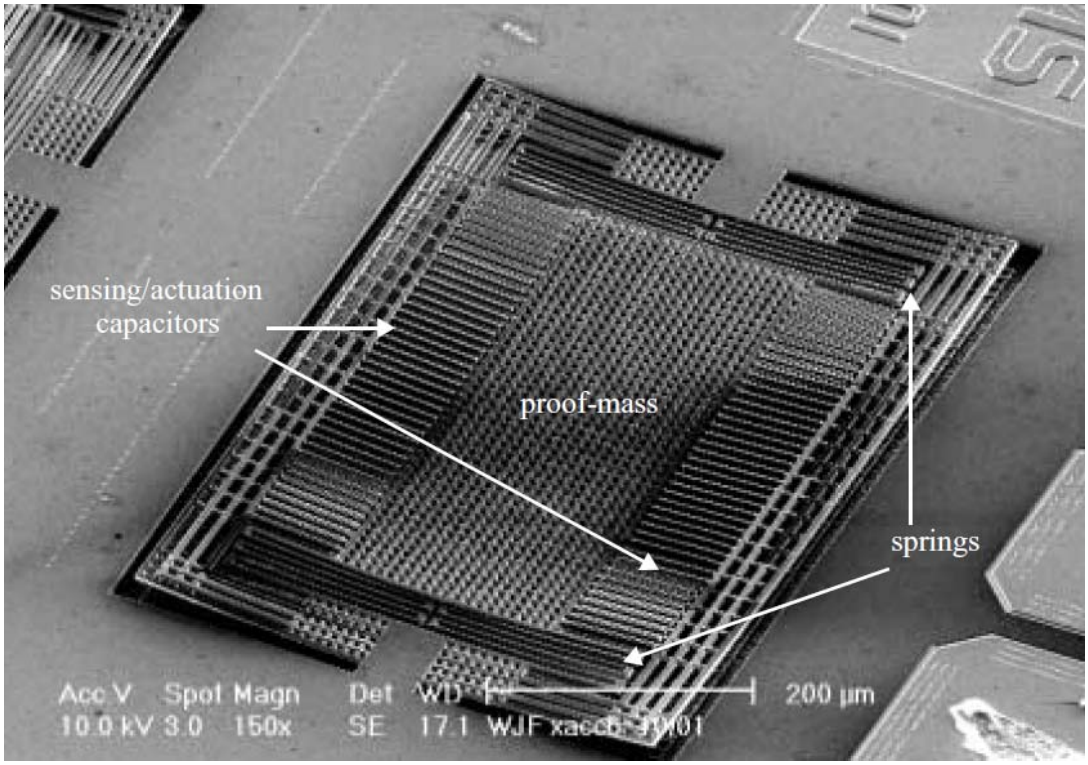

Figure 3: Scanning electron micrographs (SEM) of a CMOS MEMS accelerometer [3]

2.2 Dynamic Modeling

2.2.1 Mechanical sensing principle

Accelerometer is a transducer which transfers the acceleration into an electronic signal such as voltage, current and digital stream. We will use Newton's laws to model MEMS accelerometers. The basic mechanical structure of the accelerometer is shown in Fig 4.

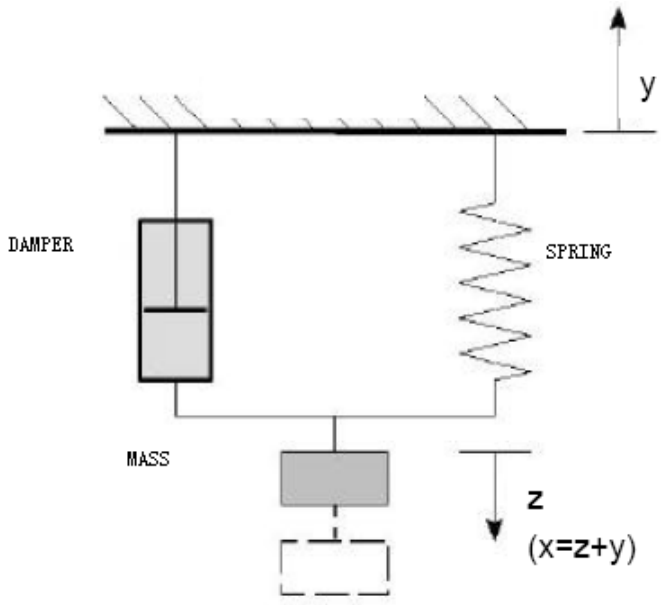

Figure 4: Mechanical model of accelerometer [11]

In Fig. 4, after the acceleration is created along *y* direction, the mass will move a distance *x* which is a relative displacement between the mass and seismic base. The whole distance that the seismic base has moved is *y*. Symbol *z* represents the absolute displacement that the mass moves. Following Newton's law, we can obtain:

$$m\ddot{z}(t)+b\dot{x}(t)+kx(t)=0$$

$$m(\ddot{x}-\ddot{y})(t)+b\dot{x}(t)+kx(t)=0$$

$$m\ddot{x}(t)+b\dot{x}(t)+kx(t)=m\ddot{y}(t)=ma(t) \qquad (2\text{-}1)$$

where m is the seismic mass, b is the damping coefficient, k is the spring constant and $a(t)$ is acceleration. The transfer function between *a(s)* and *x(s)* can be written as:

$$H(s) = \frac{x(s)}{a(s)} = \frac{1}{s^2 + \frac{b}{m}s + \frac{k}{m}} \tag{2-2}$$

We define the natural frequency ω_n and damping ratio ζ as

$$\omega_n = \sqrt{\frac{k}{m}} \qquad \zeta = \frac{b}{2\sqrt{km}} \tag{2-3}$$

The device is underdamped when ζ <1, critical damped as ζ =1 and over damped as ζ >1. Over damped accelerometer can stabilize the seismic mass. However, large damper also intensifies Brownian noise which is caused by damping effect. In this thesis, we will consider the under-damped situation, which is very common for the accelerometers in the market. We design the accelerometer to have a resonant frequency ω_n which is much larger than the expected maximum frequency of the acceleration signal. For a large ω_n, and a constant acceleration a, the quasi-static response is $x = \frac{a}{\omega_n^2}$. Therefore, the sensitivity of the accelerometer is given by

$$\frac{x(s)}{a(s)} = \frac{m}{k} = \frac{1}{\omega_n^2} \tag{2-4}$$

2.2.2 CMOS readout circuit

MEMS capacitive accelerometers are shown in Fig 5. There are two fixed electrodes and a movable seismic mass in an accelerometer. A high frequency sinusoid signal v_1 is added to the upper fixed electrode and an inversed same signal v_2 is added to the lower fixed electrode.

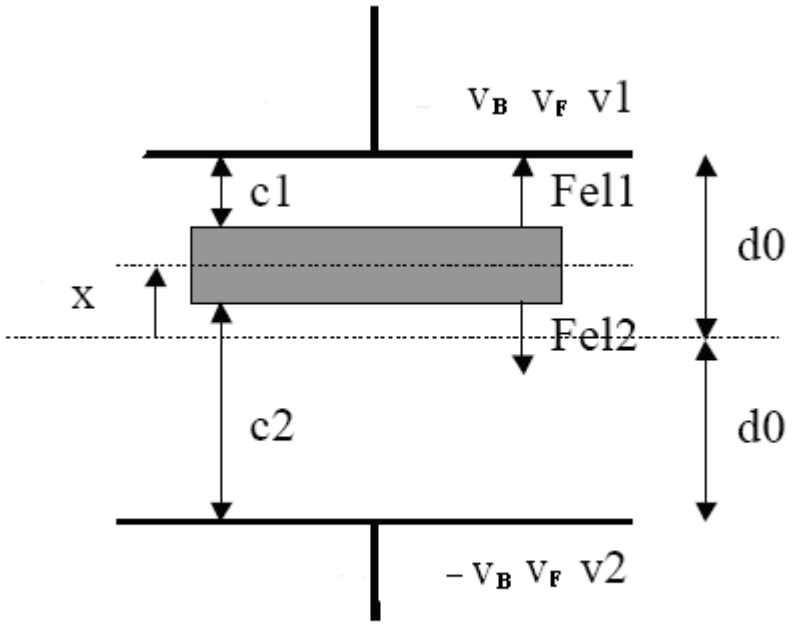

Figure 5: Accelerometer capacitor [11]

As show in Fig. 5, C_1 and C_2 are the variable sensing capacitors formed between the fixed electrodes and movable seismic mass, and x is the relative displacement between seismic mass and fixed bass. The fundamental readout circuit is shown in Fig. 6.

Assuming the operational amplifier in Fig. 6 is ideal, we will obtain the output voltage v_o (or V_{out}) as follows.

$$v_o(s) = -\frac{sC_3R_2}{1+sC_4R_2} \bullet \frac{v_1 sC_1 + v_2 sC_2}{sC_1 + sC_2 + sC_3 + 1/R_1} \tag{2-5}$$

Suppose $C_1 = C_0 + \Delta C$, $C_2 = C_0 - \Delta C$, and $v_1 = -v_2$, where C_0 is the capacitance when the movable seismic mass is in the middle of two fixed plates, ΔC is capacitance change caused by the movement of seismic mass. Equation (2-5) can be rewritten as

$$v_o(s) = -\frac{sC_3R_2}{1+sC_4R_2} \bullet \frac{2v_1 s\Delta C}{sC_1 + sC_2 + sC_3 + 1/R_1} \tag{2-6}$$

Then assume $C_3 >> C_1 + C_2$, $1/R_1 -> 0$ and $|sC_4R_2| >> 1$. Equation (2-6) can be simplified as

$$v_0(s) = -\frac{2\Delta C}{C_4} v_1(s) \tag{2-7}$$

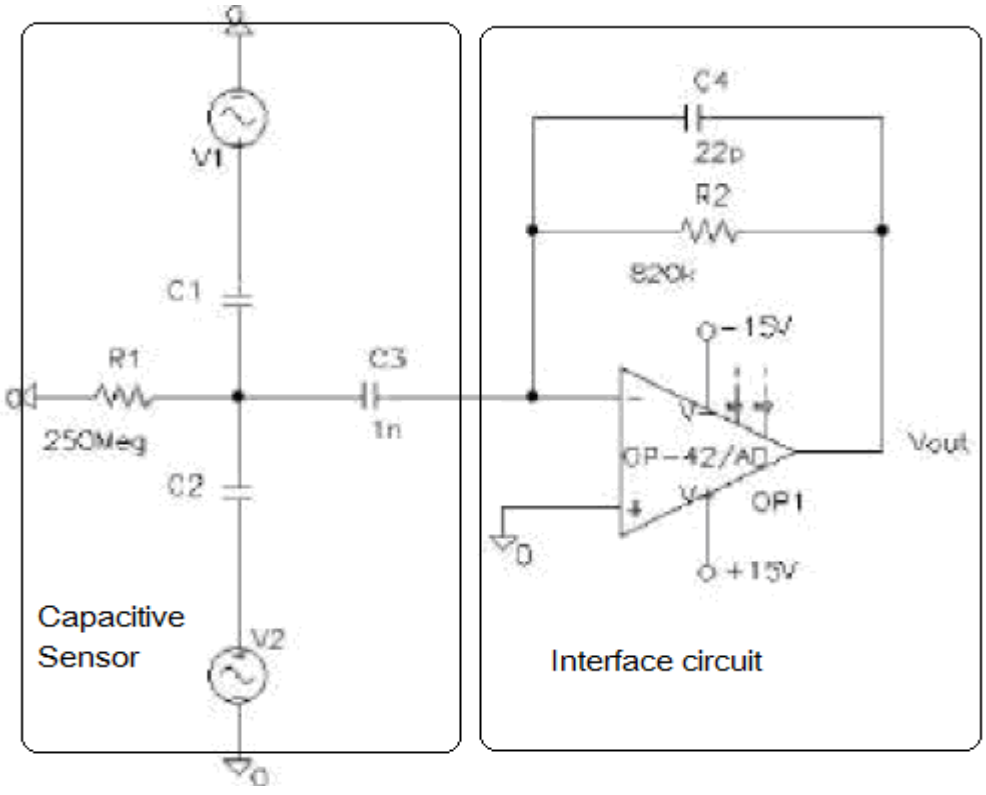

Figure 6: Readout circuit of capacitor accelerometer [10]

Based on the parallel-plate capacitor's formula, we will have:

$$2\Delta C = C_1 - C_2 = \frac{2\varepsilon_0 \varepsilon_r A x}{(d_0{}^2 - x^2)} \tag{2-8}$$

In (2-8), d_0 is the distance between fixed plate and movable seismic mass when the mass is in the middle, ε_0 is electric permittivity of vacuum, ε_r is relative dielectric constant and A is the area of the parallel plate. Then (2-7) can be written as:

$$v_0(s) = -\frac{2\varepsilon_0 \varepsilon_r A x}{C_4(d_0{}^2 - x^2)} v_1(s) \tag{2-9}$$

If assume $d_0 >> x$ the output voltage v_0 will have a linear relationship with the displacement x. The relationship can be represented by

$$v_0(s) = -\frac{2\varepsilon_0 \varepsilon_r A v_1(s)}{C_4 d_0^2} x \tag{2-10}$$

2.2.3 Electrostatic actuator

As mentioned before, two high frequency sinusoid signals are added on the both sides of fixed electrodes. Then two electrostatic forces will be produced on the seismic mass. From Fig 5, the two electrostatic forces F_{el1} and F_{el2} have same magnitudes and opposite directions as the seismic mass is in the middle. If the seismic mass is not in the middle, the electrostatic forces will have influence on the seismic mass. The electrostatic force between two parallel plates is shown in the equation below:

$$F_v = \frac{\partial E}{\partial d} = \frac{-\varepsilon_0 \varepsilon_r A}{2d^2} \cdot v^2 \tag{2-11}$$

where ε_0 is electric permittivity of vacuum, ε_r is relative dielectric constant, A is the area of the parallel plate and d is distance between the two plates. Since $v_1 = -v_2 = V_1 \sin \omega t$, we can obtain the total electrostatic force of the MEMS accelerometer capacitor structure in (2-12).

$$F_{el} = F_{el1} - F_{el2} = \frac{\varepsilon_0 \varepsilon_r A (V_1 \sin \omega t)^2}{2} \left(\frac{1}{(d_0 - x)^2} - \frac{1}{(d_0 + x)^2} \right) \qquad (2\text{-}12)$$

In (2-12), d_0 is the distance when the seismic mass is in the middle. From equation (2-12), the electrostatic force F_{el} must have the same direction as the displacement *x*, so it is always a positive feedback. The positive feedback not only has the potential to make the system unstable but also cause a big displacement of seismic mass. The big displacement of seismic mass could make the mass touch the top or bottom plate, causing the failure of operation of the accelerometer.

2.2.4 Open loop capacitive accelerometer

Now we can create an open loop model in Fig 7 by using all the information we get above.

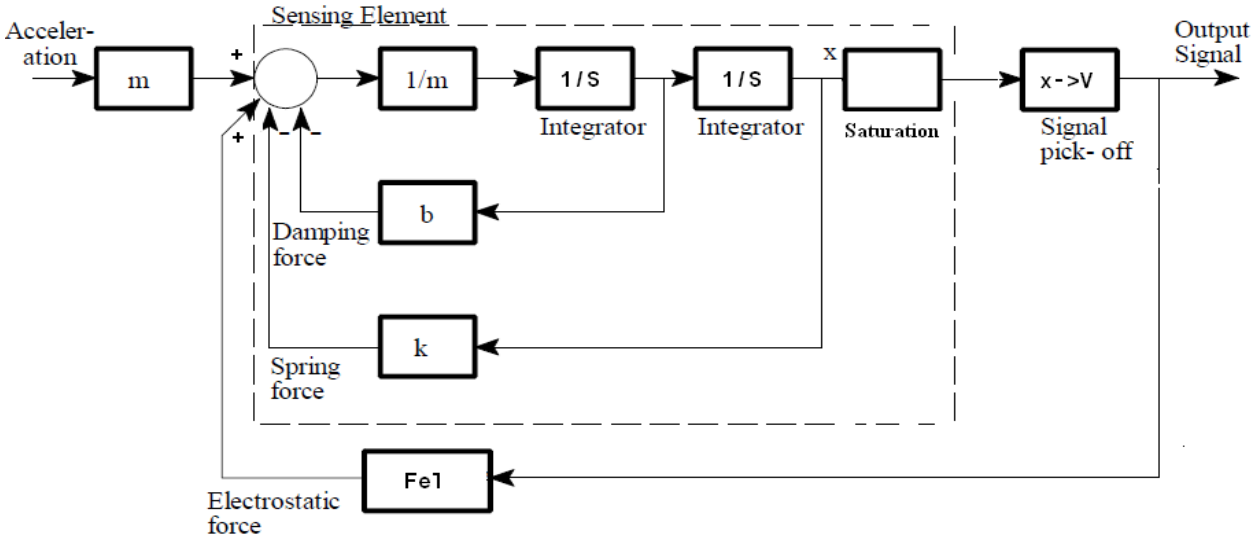

Figure 7: Open-loop capacitive accelerometer system

In Fig. 7, function $x \to V$ is based on the equation (2-10) and describes the relationship between the output voltage and displacement x. Function F_{el} is based on equation (2-12) and describes the positive feedback electrostatic force. The saturation is used to limit the maxim movement of the seismic mass. The value is equal to pull-in distance between fixed plate and movable seismic mass.

For small deflections which are caused by small acceleration and are smaller than 10^{-3} times of d_0, a constant damping coefficient can be assumed as:

$$b = \frac{2\mu E_{(W/L)} W^3 L}{d_o^2} \tag{2-13}$$

where μ is the viscosity coefficient of air, W and L are length and width of the seismic mass and $E_{(W/L)}$ is a function of the aspect ratio of the seismic mass for $W = L$, and $E_{(W/L)}$=0.42. For large deflections caused by large acceleration which is bigger than 10^{-3}

times of d_0 , the damping coefficient b becomes a function of the deflection. Its mathematical expression can be represented by

$$b(x) = \frac{1}{2}\mu A^2 \left(\frac{1}{(d_o - x)^3} - \frac{1}{(d_o + x)^3}\right) \tag{2-14}$$

All the mechanical and electronic parameters are listed in Table I [3].

Table I: Mechanical and electronic parameters

Area of seismic mass, A	$1200 \times 1550 \mu m$
viscosity of air, μ	$1.78 \times 10^{-5}\ kg/(m \times s)$
Seismic Mass, m	$3.8 \times 10^{-9} kg$
Gap, d_0	$2.3 \mu m$
Operation signal voltage, $V1$	$0.6 volt$
Operation signal frequency, f	$1 MHz$
Spring coefficient, k	$3 Nm^{-1}$
Damping coefficient, b	$7 \times 10^{-4} kgs^{-1}$ (small deflection)
Relative dielectric constant, ε_r	4
Capacitor, C_4	$20 pF$

Assume $d_0 >> x$, the Bode diagram of the open-loop capacitive accelerometer is shown in Fig. 8.

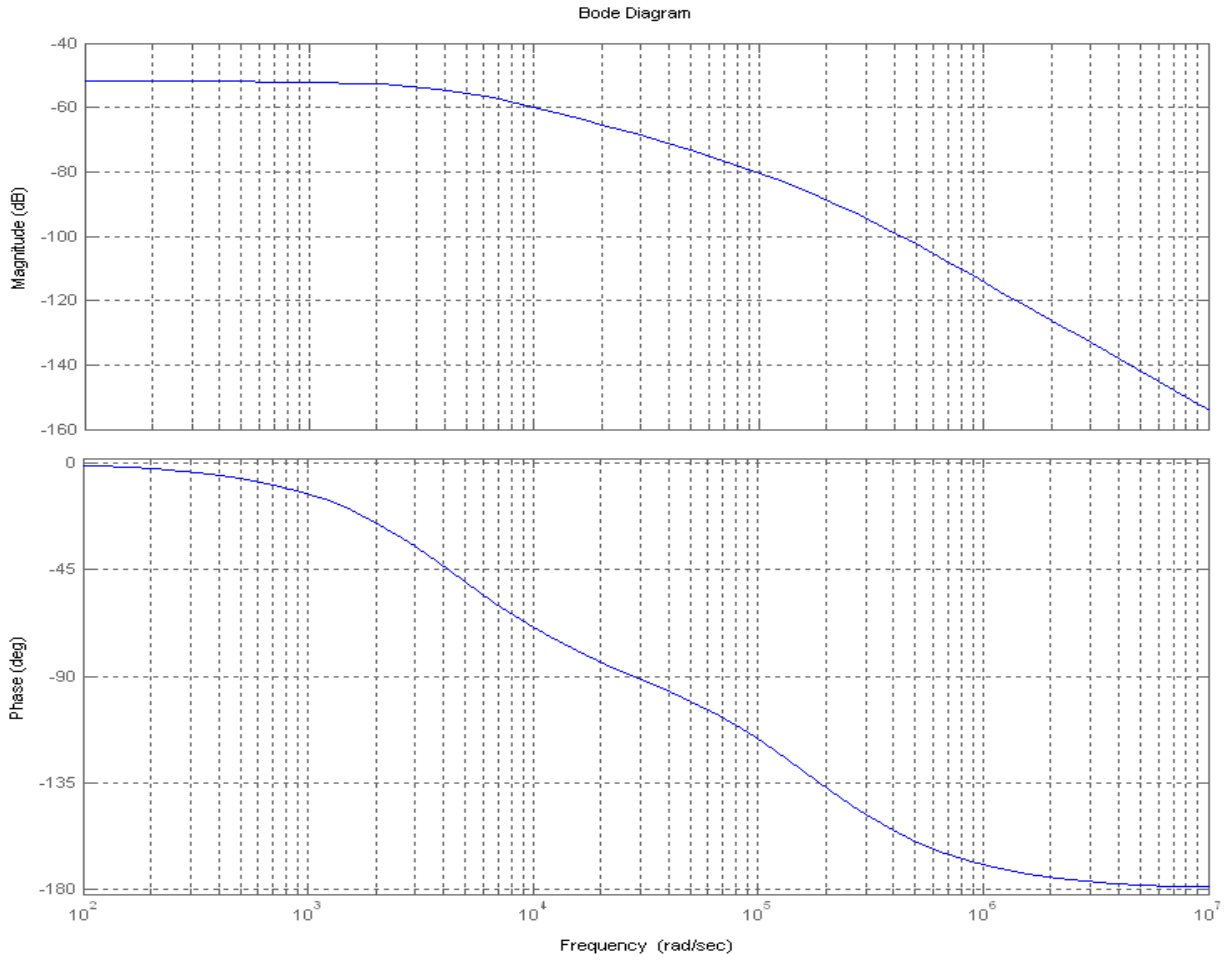

Figure 8: Frequency response of open loop capacitive accelerometer

From Fig. 8, we can see that the open-loop accelerometer has an over-damped performance and works as a low pass filter. In case of a low pass filter, the bandwidth is equal to its upper cutoff frequency at around 500 $radius/s$ or 80Hz. Fig. 8 also shows that the gain margin is close to infinity proving the open loop system is stable. The magnitude response has -50dB at maxim which is corresponding to about 10^{-7} meters of seismic mass's displacement with 10g accelerator. The relatively big value of x (which is not much smaller than d_0) makes the MEMS accelerometer system nonlinear. Also large displacement limits

the DR of high acceleration measurement. In addition the electrostatic force produces a positive feedback which can introduce instability to the accelerometer system.

2.2.5 Force-to-rebalance closed-loop MEMS accelerometer

The open-loop capacitive accelerometer design limits the bandwidth, linearity, stability and DR. Therefore a closed-loop design is needed for the accelerometer. However, the electrostatic force gives a positive feedback. How to get a negative feedback to obtain a close-loop control is the key part for controller design. A common method is adding an extra negative electrostatic force to the original open-loop system to form a negative feedback. In Fig 5, a pair of bias voltages V_B and $-V_B$ are added to the fixed beam. These bias voltages combine with the feedback voltage v_F and the driving voltages v_1 and v_2 to create new electrostatic force F_{el}' which is represented as follows:

$$F_{el}' = F_{el1}' - F_{el2}' = \frac{\varepsilon_0 \varepsilon_r A}{2}\left(\frac{(V_1 \sin \omega t - V_B + v_F)^2}{(d_0 - x)^2} - \frac{(-V_1 \sin \omega t + V_B + v_F)^2}{(d_0 + x)^2}\right) \quad (2\text{-}15)$$

Neglecting the high frequency parts and assume $d_0 >> x$, we get:

$$F_{el}' = 2\varepsilon_0 \varepsilon_r A \frac{d_0 x\left(\frac{V_1^2 + V_B^2 + v_F^2}{2}\right) - V_B d_0^2 v_F}{d_0^4} \quad (2\text{-}16)$$

Assuming the seismic mass is almost at the middle position, we can reduce (2-16) to:

$$F_{el}' = -2\varepsilon_0 \varepsilon_r A \frac{V_B v_F}{d_0^2} \quad (2\text{-}17)$$

In equation (2-17), we can see there is a linear relationship between electrostatic force F_{el}' and feedback voltage v_F . The bias voltage V_B is selected based on the dynamic range of the accelerometer. We assume the dynamic range is 10g. Then the bias voltage V_B can be obtained by follow equation:

$$V_B = \sqrt{\frac{mad_0^{\,2}}{\varepsilon_0 \varepsilon_r A}} \tag{2-18}$$

The negative feed back force F_{el}' gives the possibility to compensate the seismic mass' displacement x which is created by input acceleration and push the seismic mass back to the initial balanced middle position (x =0). This is why we name it force-to-rebalance closed-loop control.

Fig. 9 shows the force-to-rebalance closed-loop system with a proportional-integral (PI) controller.

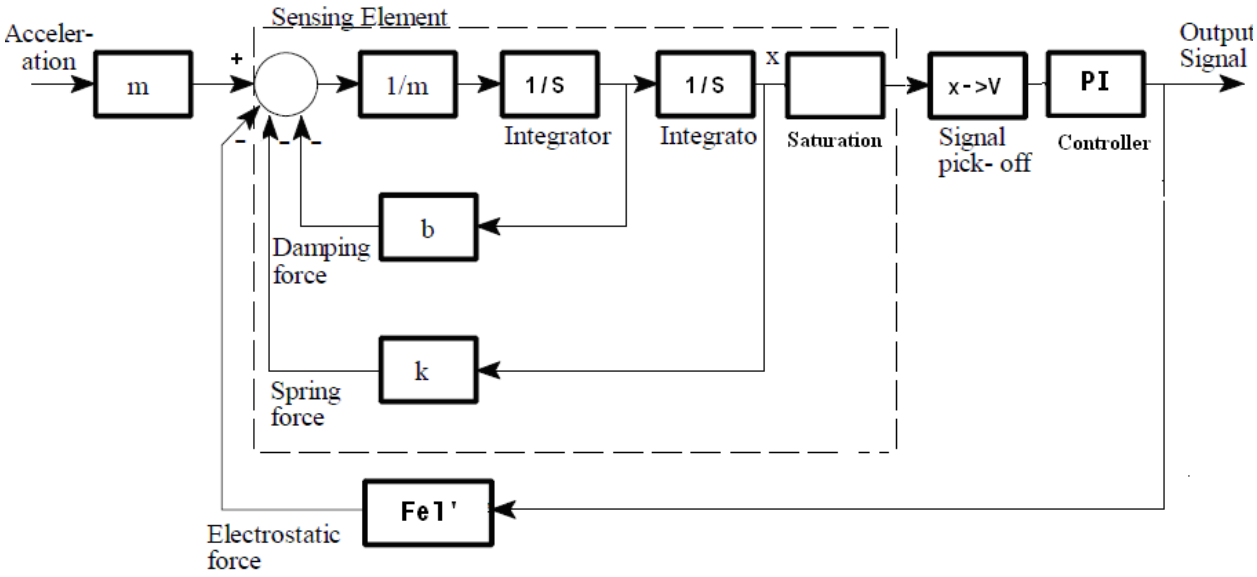

Figure 9: Closed-loop system model with a PI controller

In Fig. 9, PI controller is used to control the voltage which is added on the fixed electrodes to create the feedback force. To analyze the frequency response of the closed-loop accelerometer system, a Bode diagram was produced as shown in Fig. 10. The parameters of PI controller are chosen as Kp =10, Ki =1, where K_p represents the proportional gain, and K_i represents the integral gain for a PI controller.

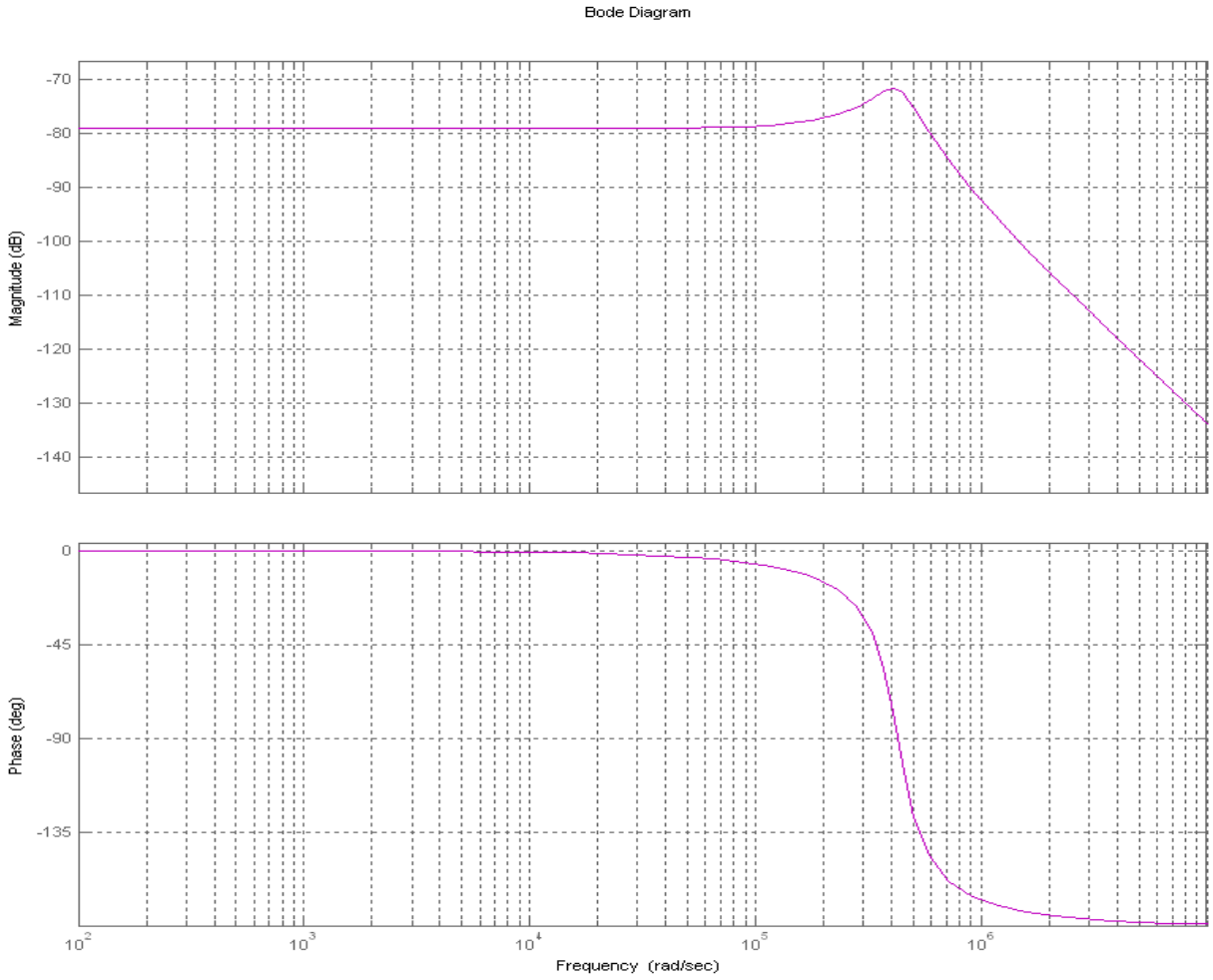

Figure 10: Frequency response of closed-loop capacitive accelerometer

From Fig 10, the bandwidth of the system is increased from 80 *Hz* for (open-loop system) to 80 *KHz* as expected. As an accelerometer, large bandwidth can track acceleration with large frequency range. The bandwidth up to 80 *KHz* would be sufficient for the performance of recent accelerometers. However, the large bandwidth could also be easily influenced by

noise. In Fig. 10, the magnitude for the closed-loop system is lower than the one for open-loop system. The low magnitude makes the displacement of seismic mass smaller and it also makes the system more linear. In addition, the lower magnitude leads to high system sensitivity which is about $1\,mV/g$ and increases the DR of the system. However, the high sensitivity also easily increases the SNR of the system.

2.3 Summary of this chapter

In this chapter, the modeling of a typical surface micromachining accelerometer, including sensing principle and electronic readout circuit is introduced. With this modeling open-loop and force-to-re-balance closed-loop MEMS accelerometers are discussed. Based upon the frequency response, the closed-loop system shows a larger bandwidth, more linearity, more DR and more stability than the open-loop system.

.

CHAPTER III

NOISE CONSIDERATION

Brownian noise and electronic noise are two main causes that degrade the performance of MEMS accelerometers. The complete analyses of these noises are conducted to successfully design a more reliable MEMS accelerometer with better sensitivity and large SNR [13]. In this chapter, we will study the Brownian and electronic noises and their effects on the MEMS accelerometer.

3.1 Brown noise and electronic noise

3.1.1 Brown noise

Brownian noise is thermal-mechanical noise. It creates a random force with Brownian motion of air molecules caused by damping and is directly applied to seismic mass. The power spectral density (PSD) of the Brownian noise force is shown in (3-1):

$$\overline{F_B^2}(f) = 4k_B T b \tag{3-1}$$

In (3-1), F_B is the Brownian noise force, k_B is Boltzman constant, T is absolute temperature and b is damping coefficient. From (3-1), the bigger the damping coefficient is, the more the Brownian noise we have. To reduce the Brownian noise, small damping coefficient is anticipated. However, small damping coefficient causes small damping ratio that makes the MEMS accelerometer work at under-damped condition. The under-damped condition could make the mass in accelerometer oscillate. Equation (3-1) also shows the Brownian noise is a white noise which has a zero mean and F_B^2 variance.

The accelerometer's noise performance is determined by acceleration-referred noise floor. Brownian noise could produce the following acceleration from Newton's law.

$$\overline{a_B^2}(f) = \frac{\overline{F_B^2}}{m^2} = \frac{\sqrt{4k_B Tb}}{g^2 m^2} \; g^2 / Hz \qquad (3\text{-}2)$$

The thermal-mechanical Brownian noise floor is between $10 \sim 100 \mu g / rtHz$ .This noise affects the process of system. So we consider it as process noise.

3.1.2 Electronic noise

In Fig 6, the readout circuit of capacitive accelerometer can be divided into two parts: capacitive sensor part and interface circuit part. From (3-3), capacitive sensor part has high impedance about $10^7 \Omega$ when operating frequency f is $1MHz$. The symbol Z is the impedance of the sensor part, C is the sensing capacitance formed between the fixed electrodes and the movable seismic mass. To match this high impedance output, a high-impedance input MOSFET is used in interface circuit.

$$Z = \frac{1}{2\pi fC} \tag{3-3}$$

Fig 11 shows three major electronic current noises in a MOSFET: input MOSFET thermal noise, input MOSFET flicker noise and diode leakage noise. The capacitor C_p is the parasitic capacitor, and C_{gd} and C_{gs} are gate-to-drain and gate-to-source capacitors.

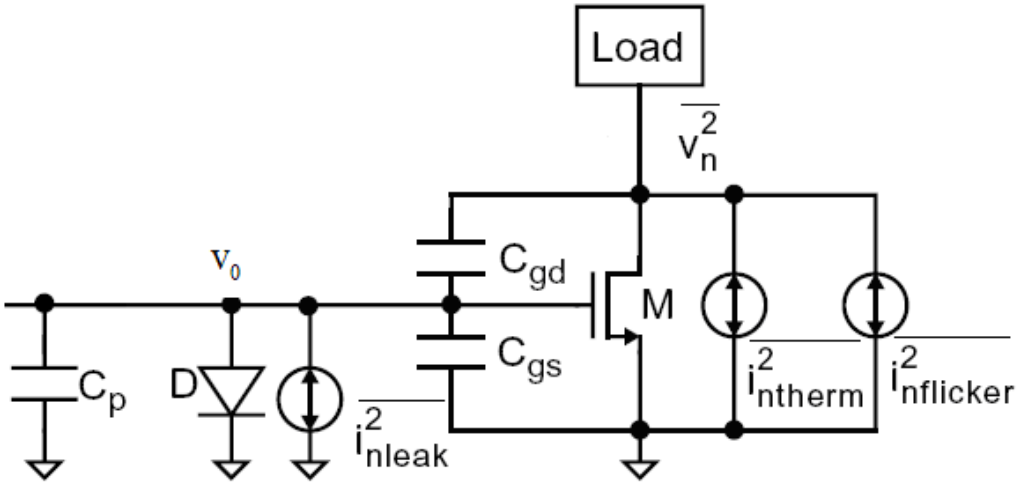

Figure 11: Thermal, flicker and leak current noises of MOSFET [12]

Assuming long transistor channel, the PSD of three noises are given by the following equations [12]:

$$\overline{i_{ntherm}^2}(f) = 4\gamma k_B T g_m = 4\gamma k_B T \sqrt{2\mu_n C_{ox}(W/L) I_D} \tag{3-4}$$

$$\overline{i_{nflicker}^2}(f) = \frac{K_f I_D}{C_{ox} L^2 f} \tag{3-5}$$

$$\overline{i_{nleak}^2}(f) = 2qI_{leak} \tag{3-6}$$

In (3-4), (3-5) and (3-6), $\overline{i_{ntherm}^2}(f)$, $\overline{i_{nflicker}^2}(f)$ and $\overline{i_{nleak}^2}(f)$ are MOSFET thermal noise, MOSFET flicker noise and diode leakage noise in term of current, γ is the thermal noise coefficient, g_m is transconductance, μ_n is carrier mobility, C_{ox} is the gate capacitance per

unit area, W and L are the MOSFET channel width and length, I_D is the bias current, K_f is flicker noise coefficient, f is the circuit operating frequency, q is the electron charge, and I_{leak} is the diode leakage current.

Then we can get the electronic noises in terms of voltage $\overline{v_{ntherm}^2}(f)$, $\overline{v_{nflicker}^2}(f)$ and $\overline{v_{nleak}^2}(f)$ as follows.

$$\overline{v_{ntherm}^2}(f) = \overline{i_{ntherm}^2} / g_m^2 = \frac{4\gamma k_B T}{g_m} = \frac{4\gamma k_B T}{\sqrt{2\mu_n C_{ox}(W/L) I_D}} \tag{3-7}$$

$$\overline{v_{nflicker}^2}(f) = \overline{i_{nflicker}^2} / g_m^2 = \frac{K_f I_D}{C_{ox} L^2 f g_m^2} = \frac{K_f}{2\mu_n C_{ox}^2 WLf} \tag{3-8}$$

$$\overline{v_{nleak}^2}(f) = \frac{\overline{i_{nleak}^2}}{(2\pi C_{total} f)^2} = \frac{qI_{leak}}{(2\pi C_{total} f)^2} \tag{3-9}$$

In (3-9), C_{total} is the total capacitance of the whole readout circuit including the sensor part and interface circuit. For the capacitive MEMS accelerometer which detects the signal by using capacitive dividers, the parasitic capacitor C_p can degrade sensitivity. To reduce the effects of parasitic capacitors, small-size MOSFET is anticipated. However, from (3-7), (3-8) and (3-9), all of the three electronic noises are inversely proportional to the capacitances and the size of the MOSFET. The PSD of the total output noise voltage is

$$\begin{aligned} \overline{v_n^2} &= \overline{v_{ntherm}^2}(f) + \overline{v_{nflicker}^2}(f) + \overline{v_{nleak}^2}(f) \\ &= \frac{4\gamma k_B T}{\sqrt{2\mu_n C_{ox}(W/L) I_D}} + \frac{K_f}{2\mu_n C_{ox}^2 WLf} + \frac{qI_{leak}}{(2\pi C_{total} f)^2} \end{aligned} \tag{3-10}$$

We can get the open-loop voltage-referred electronic noise floor as shown in Fig 12.

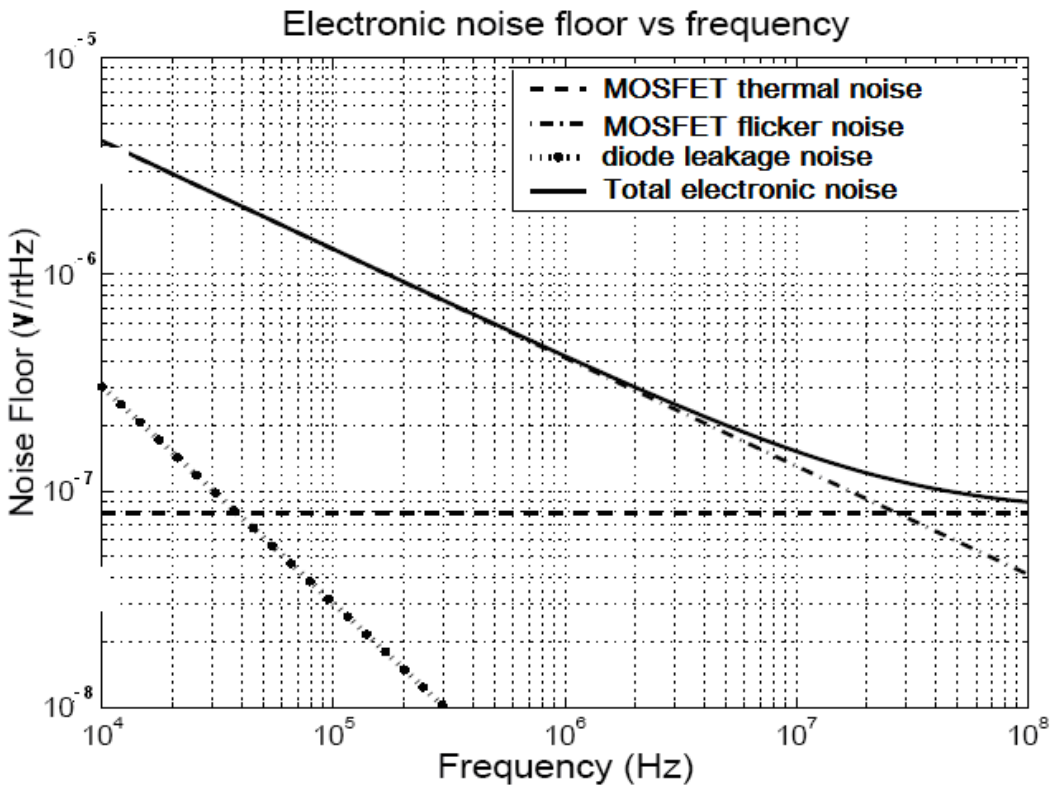

Figure 12: Voltage -referred electronic noise floor versus frequency

With a constant circuit's operating frequency, the noise voltage can be determined as a random noise with zero mean and variance of $\overline{v_n^2}$. Combining (3-10), (2-7) and (2-12), we can also get the acceleration-referred electronic noise around $20\mu g/rtHz$. As the circuit's operation frequency is 1 *MHz*, the acceleration-referred electronic noise is $0.02g$ which is close to $0.2m/s^2$. Since this acceleration-referred electronic noise affects the measurement result of accelerometer system, we will consider it as measurement noise.

3.2 Noise performance in open-loop and closed-loop system

Based on the information from section 3.1, we can get the closed-loop model shown in Fig. 13.

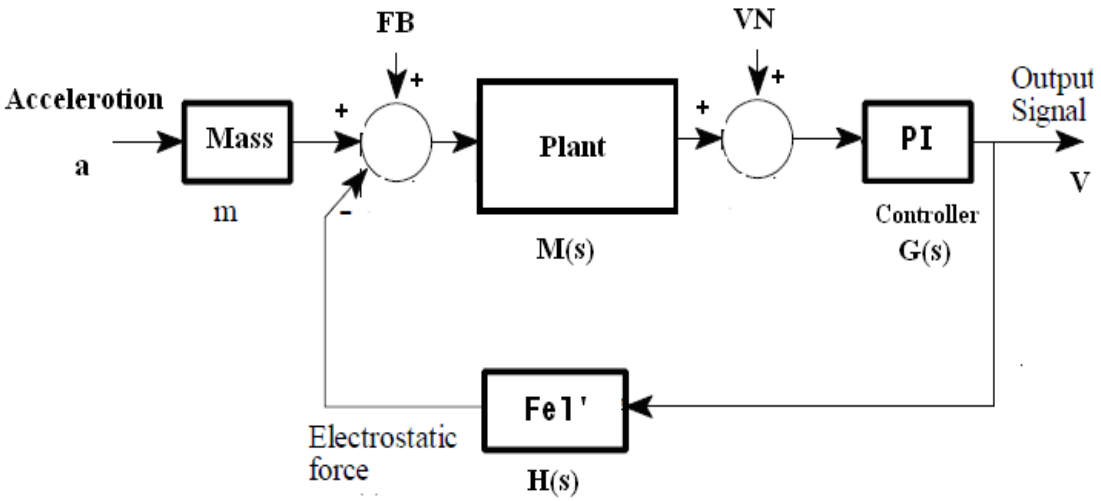

Figure 13: Closed-loop accelerometer model with Brownian and electronic noises

As shown in Fig. 13, the Brownian noise F_B is added to the system as a random force and the electronic noise V_N is added to the system output as a random voltage. As we discussed in chapter 2, for a real MEMS accelerometer, the PI controller can not control force error directly. However, voltage signal can be measured and used as feedback signal to create electrostatic force F_{el}'. PI controller in Fig. 13 is used to control the feedback voltage signal. The output equation of the closed-loop system can be obtained through following equation development.

$$V(s) = [(ma + F_B - H(s)V(s))M(s) + V_N]G(s)$$

$$(1 + H(s)M(s)G(s))V(s) = mM(s)G(s)a + F_B M(s)G(s) + V_N G(s)$$

$$V(s) = \frac{M(s)G(s)ma}{1 + H(s)M(s)G(s)} + \frac{F_B M(s)G(s)}{1 + H(s)M(s)G(s)} + \frac{V_N G(s)}{1 + H(s)M(s)G(s)} \qquad (3\text{-}11)$$

In (3-11), the output $V(s)$ has three inputs: acceleration a, Brownian noise F_B and electronic noise V_N. Then we can get the SNR (B) between Brownian noise and acceleration and SNR (E) between electronic noise and acceleration. They are given by (3-12) and (3-13).

$$SNR(B) = \frac{\dfrac{M(s)G(s)ma}{1+H(s)M(s)G(s)}}{\dfrac{F_B M(s)G(s)}{1+H(s)M(s)G(s)}} = \frac{ma}{F_B} \tag{3-12}$$

$$SNR(E) = \frac{\dfrac{M(s)G(s)ma}{1+H(s)M(s)G(s)}}{\dfrac{V_N G(s)}{1+H(s)M(s)G(s)}} = \frac{M(s)ma}{V_N} \tag{3-13}$$

Based on the open-loop system model in Fig 7, we get a new open-loop model with Brownian and electronic noises as shown in Fig14. In Fig. 14, V_1 is output signal of accelerometer before measurement noise is added.

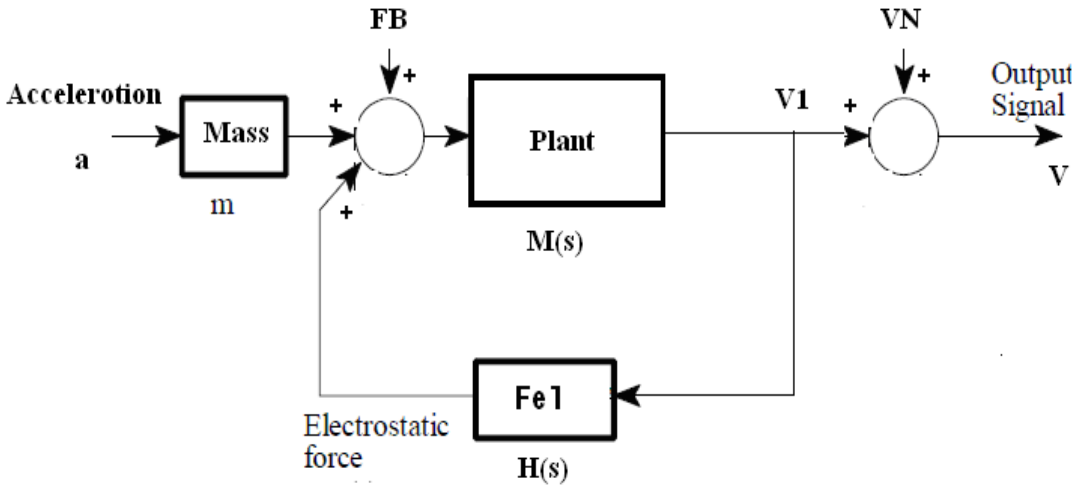

Figure 14: Open-loop model with Brownian and electronic noises

The output equation of the open-loop system can be obtained from equation (3-14) and (3-15).

$$\begin{aligned} V1(s) &= (ma + F_B + H(s)V1(s))M(s) \\ &= M(s)ma + M(s)F_B + M(s)H(s)V1(s) \\ &= \frac{M(s)ma + M(s)F_B}{1 - M(s)H(s)} \end{aligned} \tag{3-14}$$

$$\begin{aligned} V(s) &= V1(s) + V_N \\ &= \frac{M(s)ma}{1 - M(s)H(s)} + \frac{M(s)F_B}{1 - M(s)H(s)} + V_N \end{aligned} \tag{3-15}$$

Then, same as the closed-loop system, we can get the SNR (B) between Brownian noise and acceleration and SNR (E) between electronic noise and acceleration. They are given by (3-16) and (3-17)

$$SNR(B) = \frac{M(s)ma}{M(s)F_B} = \frac{ma}{F_B} \tag{3-16}$$

$$SNR(E) = \frac{M(s)ma}{(1 - M(s)H(s))V_N} \tag{3-17}$$

Comparing (3-16) with (3-12), (3-17) with (3-13) (the equations about SNR), we can see that the SNRs for Brownian noise are same for both open-loop and closed-loop systems. In (3-17), the term $1 - M(s)H(s)$ is always smaller than 1. So the SNR (E) of open-loop system is larger than that of closed-loop system. The noise performance is worse in force-to-rebalance closed-loop feedback control with PI controller than the one for open-loop system..

3.3 Summary of this chapter

In this chapter, we analyzed two major noise sources that are thermal-mechanical and electronic noises. The thermal-mechanical noise which we considered as a process noise is between $10 \sim 100 \mu g / rtHz$ and the electronic noise which we considered as a measurement noise is above $20 \mu g / rtHz$ while the electronic circuit is operating at the frequency of $1 MHz$. In addition, we found that the SNR for electronic noise is worse in the closed-loop MEMS accelerometer system than the one in open-loop configuration. In order to reduce the influence of noise, a new sensing and control method has to be found to replace the traditional PI controller and to improve the SNR in closed-loop accelerometer system.

CHAPTER IV

KALMAN FILTER AS OBSERVER

This chapter discusses the design of a Kalman filter for MEMS accelerometers. We start our discussion with a quick review of what is an observer and what is a Kalman filter observer. Then we will prove the properties of Kalman filter and give a basic concept of discrete time Kalman filter. Finally we will give a quick overview of hybrid extended Kalman filter which we can use to perform a noiseless MEMS accelerometer.

4.1 Observer

Estimation of immeasurable state variables is called observation. A device that observes the states is called state-observer or just observer [14]. Open-loop and Closed-loop observers are two basic types of observers. In this thesis, we will use closed-loop observer which can drive the estimated states to the actual states if the observer parameters are properly designed. Closed-loop observers can improve the robustness of a system against parameter uncertainties and noise. Filter can estimate useful information from noise measurements. In

frequency-domain, filtering is used to separate the frequency response of useful signal from that of noise. The Kalman filter (KF) is a special type of observer based on the knowledge of statistics for both process and measurement noise.

There are two types of commonly used observers, Luenberger and Kalman observers. Luenberger observer is based upon the fact that the system is deterministic. Kalman Filter is stochastic type. The basic Kalman filter is only applied to linear stochastic systems while extended Kalman filter (EKF) can be used on non-linear systems. For continuous-time non-linear systems with discrete-time measurements, a hybrid EKF will be employed.

We can describe a linear time-invariant system in the following state equation (4-1):

$$\begin{aligned} \dot{x}(t) &= Ax(t) + Bu(t) \\ y(t) &= Cx(t) \end{aligned} \tag{4-1}$$

In (4-1), matrices A, B, and C represent state matrix, input matrix, and output matrix respectively. If this system is observable, state estimation $\hat{x}(t)$ can be obtained based on the input $u(t)$ and output $y(t)$ with the knowledge of A, B and C. A feedback based on the difference between the plant output and observer output is added to the input of observer. The observer equation given by:

$$\begin{aligned} \dot{\hat{x}}(t) &= A\hat{x}(t) + Bu(t) + L(y(t) - \hat{y}(t)) \\ \hat{y}(t) &= C\hat{x}(t) \end{aligned} \tag{4-2}$$

Define the estimation error as $e(t) = x(t) - \hat{x}(t)$. Then we will have

$$\dot{e}(t) = (A - LC)e(t) \tag{4-3}$$

In (4-3), if L can be designed (via pole placement method) to make the above equation stable, estimation error $e(t)$ will converge to zero no matter what the initial condition of *x(t)*

is. Equation (4.2) is a basic Luenberger observer which is applicable to linear, time-invariant deterministic systems.

4.2 Kalman Filter

4.2.1 Introduction

With the development of digital computing, Kalman filters have been introduced to academic research and industrial application in many fields. Success in the areas of aeronautics and aerospace engineering in 1960's made the Kalman filter popular [15]. The Kalman Filter is a recursive solution for the linear filtering problem which is estimating the states of a linear system from output measurements linearly related to estimating states but influenced by Gaussian white noise. Kalman Filter is an optimal estimator according to a quadratic function of the estimation errors between real states and observed states.

Mathematically, Kalman Filter is a set of equations which give a combination of recursive least square method [15] and propagation of states and covariance. There are two different noise sources that are process noise and measurement noise. Recursive lease square method deals with the measurement noise and propagation of states and covariance, and hence reduce the effect of process noise. The performance of Kalman Filter is excellent in several aspects. It can give estimation of the past, the current and the future states even without knowing the precise value of the parameters of the modeled system. When applied to a physical system, Kalman Filter works as an extremely effective method which uses noisy sensor outputs to estimate uncertain dynamic system states.

4.2.2 Property of Kalman Filter

Consider a Linear Time Invariant (LTI) system in following equation:

$$\begin{aligned} \dot{x}(t) &= Ax(t) + Bu(t) + w(t) \\ y(t) &= Cx(t) + v(t) \end{aligned} \tag{4-4}$$

where $w(t)$ is process noise and $v(t)$ is measurement noise. There are three following assumptions that need to be made before we design the Kalman filter.

(1) (A, C) is observable.

(2) $w(t)$ and $v(t)$ are independent white noises, their expect value $E[v(t)] = E[w(t)] = 0$, their autocorrelation $E[w(t)w^T(\tau)] = Q\delta(t-\tau)$ and $E[v(t)v^T(\tau)] = R\delta(t-\tau)$ are positive semidefined. That means $Q = Q^T \geq 0$ and $R = R^T \geq 0$.

(3) $\left(A, Q^{1/2}\right)$ is stable.

Same as our discussion of the Luenberger observer before, Kalman filter is used to design a state observer to estimate the state $x(t)$ by $\hat{x}(t)$, such that the cost function J_e (given by (4-5)) is minimized.

$$J_e = E[(x(t) - \hat{x}(t)^T (x(t) - \hat{x}(t))] \tag{4-5}$$

The dynamic equation of steady state Kalman Filter is as follow:

$$\begin{aligned} \dot{\hat{x}} &= A\hat{x} + Bu + K_k(y - \hat{y}) \\ \hat{y} &= C\hat{x} \end{aligned} \tag{4-6}$$

In equation (4-6), K_k is Kalman gain which is given as:

$$K_k = P_e C^T R^{-1} \tag{4-7}$$

where P_e is the positive definite solution of Riccati equation:

$$P_e A^T + A P_e - P_e C^T R^{-1} C P_e + Q = 0 \tag{4-8}$$

If initial state $\hat{x}(0)$ is given and $e = x - \hat{x}$, Kalman filter has two major properties [16]:

(1) $$\lim_{t\to\infty} E[e(t)] = \lim_{t\to\infty} E[x(t) - \hat{x}(t)] = 0 \tag{4-9}$$

(2) $$\lim_{t\to\infty} J_e = \lim_{t\to\infty} E[e(t)^T e(t)] = trace\ P_e \tag{4-10}$$

The proof of the properties of Kalman Filter is given as follows. Recall (4-4) and (4-6), we can get

$$\begin{aligned} \dot{e} &= \dot{x} - \dot{\hat{x}} = Ax + Bu + w(t) - A\hat{x} - Bu - K_k[Cx + w(t) - C\hat{x}] \\ &= (A - K_k C)(x - \hat{x}) + w(t) - K_k v(t) \\ &= (A - K_k C)e + [I - K_k]\begin{pmatrix} w(t) \\ v(t) \end{pmatrix} \end{aligned} \tag{4-11}$$

Here we define $A - K_k C = \overline{A}$ and $[I - K_k]\begin{pmatrix} w(t) \\ v(t) \end{pmatrix} = d(t)$, then we get

$$\dot{e} = \overline{A} e + d(t) \tag{4-12}$$

$$e(t) = e^{\overline{A}t} \cdot e(0) + \int_0^t e^{\overline{A}(t-\tau)} d(\tau) \cdot d\tau \tag{4-13}$$

Then the covariance of estimation error $P(t)$ is obtained by

$$
\begin{aligned}
P(t) = E[e(t)e^T(t)] &= E[(e^{\bar{A}t}\cdot e(0) + \int_0^t e^{\bar{A}(t-\tau)}d(\tau)\cdot d\tau)\cdot(e^{\bar{A}t}\cdot e(0) \\
&\quad + \int_0^t e^{\bar{A}(t-\tau)}d(\tau)\cdot d\tau)^T] \\
&= e^{\bar{A}t}E[e(0)e^T(0)]e^{\bar{A}^T t} + \int_0^t e^{\bar{A}(t-\tau)}E[d(\tau)e^T(0)]e^{\bar{A}^T t}\cdot d\tau \\
&\quad + \int_0^t e^{\bar{A}t}E[e(0)d^T(t)]\, e^{\bar{A}^T(t-\tau)}\cdot d\tau \\
&\quad + \int_0^t e^{\bar{A}(t-\tau)}d\tau \int_0^t E[d(\tau)d^T(\sigma)]\, e^{\bar{A}^T(t-\sigma)}\cdot d\sigma
\end{aligned}
\tag{4-14}
$$

Assume the initial error $e(0)$ and $d(t)$ are independent of each other. Then $E[e(0)d^T(t)] = 0$. Recall (4-7) and (4-8), we can get:

$$
\begin{aligned}
&P_e A^T - P_e C^T R^{-1} C P_e + A P_e - P_e C^T R^{-1} C P_e + P_e C^T R^{-1} C P_e + Q = 0 \\
&P_e(A^T - C^T K_k^{\ T}) + (A - K_k C)P_e + K_k R K_k^T + Q = 0
\end{aligned}
\tag{4-15}
$$

As we defined before, $A - K_k C = \bar{A}$. Then (4-15) is rewritten as

$$
P_e \bar{A}^T + \bar{A} P_e = -K_k R K_k^T - Q = \nabla \tag{4-16}
$$

In (4-16), ∇ is obtained from the autocorrelation of $d(t)$:

$$
\begin{aligned}
E[d(t)d^T(\tau)] &= [I - K_k]\begin{pmatrix} E[w(t)w^T(\tau)] & E[w(t)v^T(\tau)] \\ E[v(t)w^T(\tau)] & E[v(t)v^T(\tau)] \end{pmatrix}\begin{bmatrix} I \\ -K_k^T \end{bmatrix} \\
&= [I - K_k]\begin{pmatrix} Q\delta(t-\tau) & 0 \\ 0 & R\delta(t-\tau) \end{pmatrix}\begin{bmatrix} I \\ -K_k^T \end{bmatrix} \\
&= (Q + K_k R K_k^T)\delta(t-\tau) \\
&= \nabla\delta(t-\tau)
\end{aligned}
\tag{4-17}
$$

Since $Q = Q^T \geq 0$, we will have $\nabla = Q + K_k R K_k^T \geq 0$. Assuming $\left(A, Q^{1/2}\right)$ is stabilizable, the matrix $\bar{A} = A - K_k C$ will be asymptotically stable. As $t \to \infty$, we get $e^{\bar{A}t} \to 0$. Recall the (4-13), we can get first property (4-9) approved. Now (4-14) can be transformed to:

$$
\begin{aligned}
P(\infty) &= \int_0^\infty e^{\bar{A}(t-\tau)} d\tau \int_0^t E[d(\tau) d^T(\sigma)]\, e^{\bar{A}^T(t-\sigma)} \cdot d\sigma \\
&= \int_0^\infty e^{\bar{A}(t-\tau)} d\tau \nabla e^{\bar{A}^T(t-\tau)} \cdot d\tau \\
&= \int_0^\infty e^{\bar{A}\pi} d\tau \nabla e^{\bar{A}^T\pi} \cdot d\pi
\end{aligned}
\tag{4-18}
$$

Then we need to prove $P(\infty) = P_e$ which is the solution of Kalman filter Riccati equation (4-8). Assume $\dot{z} = \bar{A}^T z$ and initial condition $z(0)$ is given, we get $z(t) = e^{\bar{A}t} z(0)$ and $z(\infty) = 0$.

Now in view of equation (4-16), we have:

$$
\begin{aligned}
& P_e \bar{A}^T + \bar{A} P_e = -\nabla \\
& z^T [P_e \bar{A}^T + \bar{A} P_e] z = -z^T \nabla z \\
& z^T P_e \dot{z} + \dot{z}^T P_e z = -z^T \nabla z \\
& \frac{d}{dt}(z^T P_e z) = -z^T \nabla z
\end{aligned}
\tag{4-19}
$$

Next, we integrated both sides of (4-19) to obtain:

$$
\begin{aligned}
\int_0^\infty -z^T \nabla z \, dt &= \int_0^\infty z^T(0) e^{\bar{A}^T t} \nabla e^{\bar{A}t} z(0) dt \\
&= z^T(0) [\int_0^\infty e^{\bar{A}^T t} \nabla e^{\bar{A}t} dt] z(0) \\
&= z^T(0) P(\infty) z(0)
\end{aligned}
\tag{4-20}
$$

$$
\begin{aligned}
\int_0^\infty \frac{d}{dt}(z^T P_e z) dt &= z^T(t) P_e z(t) \Big|_0^\infty \\
&= z^T(0) P_e z(0)
\end{aligned}
\tag{4-21}
$$

Thus, from (4-20) and (4-21) we can get:

$$
P(\infty) = P_e \tag{4-22}
$$

Now recall the (4-18), we can proof the second property (4-10).

Finally we approve the properties of Kalman filter shown in equations (4-9) and (4-10). Kalman filter can be used to design a state observer to estimate the state $x(t)$ by $\hat{x}(t)$, such that the estimation error $e \to 0$ as $t \to \infty$ and the cost function J_e is minimized [16].

4.2.3 Discrete Time Kalman Filter

We can use Kalman Filter to estimate the state $x_{(k)} \in R^n$ of a discrete-time system as well. A discrete-time system is described in following equation:

$$\begin{aligned} x_{(k+1)} &= F_{(k)}x_{(k)} + G_{(k)}u_{(k)} + w_{(k)} \\ y_{(k)} &= H_{(k)}x_{(k)} + v_{(k)} \end{aligned} \tag{4-23}$$

where $w_{(k)}$ is the process noise and $v_{(k)}$ is the measurement noise. $w_{(k)}$ and $v_{(k)}$ are white, zero-mean, uncorrelated white noise with covariance Q_k and R_k respectively. Matrix $F_{(k)}$ gives the relationship of the states from step time kT (T is sampling time and $T=t_k - t_{k-1}$) to step time $(k+1)T$. Matrix $G_{(k)}$ relates the control input u to state x. Matrix $H_{(k)}$ relates state to measurement $y_{(k)}$ .Matrices $F_{(k)}$, $G_{(k)}$ and $H_{(k)}$ are discretized from continuous dynamic system matrices A, B and C in equation (4-1). The mathematical expressions for $F_{(k)}$, $G_{(k)}$, and $H_{(k)}$ are given in (4-24). The mathematical expressions for ω_k and v_k and their covariance are given by (4-25).

$$\begin{aligned} F_{(k)} &= e^{AT} \\ G_{(k)} &= \int_{t_k}^{t_{k-1}} e^{A(t-\tau)} Bu(\tau) d\tau \\ H_{(k)} &= C \end{aligned} \tag{4-24}$$

$$
\begin{aligned}
&w_k \sim (0, Q_k) \\
&v_k \sim (0, R_k) \\
&E[w_k w_j^T] = Q_k \delta_{k-j} \\
&E[v_k v_j^T] = R_k \delta_{k-j} \\
&E[v_k w_j^T] = 0
\end{aligned}
\tag{4-25}
$$

A posteriori state estimation is represented by $\hat{x}_k^+$. A priori state estimation is represented by $\hat{x}_k^-$. We defined P_k^- as the covariance of the state estimation error of $\hat{x}_k^-$ and P_k^+ as the covariance of the state estimation error of $\hat{x}_k^+$. Then we will have

$$
\begin{aligned}
P_k^- &= E[(x_k - \hat{x}_k^-)(x_k - \hat{x}_k^-)^T] \\
P_k^+ &= E[(x_k - \hat{x}_k^+)(x_k - \hat{x}_k^+)^T]
\end{aligned}
\tag{4-26}
$$

Kalman filter algorithm can be described as a recursive feedback loop between time update equations and measurement update equations. As shown in Fig 15, the time update equations produce a priori estimate for the state in next time step from the current state and error covariance. The measurement update equations add a new measurement to the priori estimate of the next step to obtain a corrected posterior estimate.

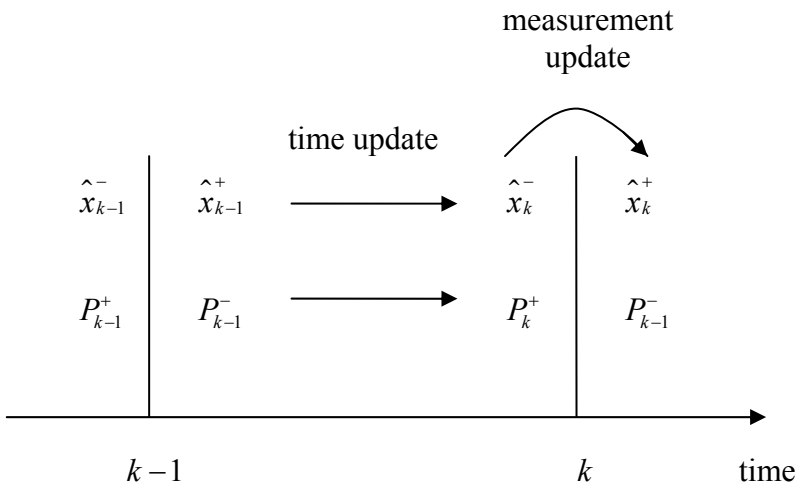

Figure 15: On-going timeline of a priori and a posteriori state and covariance estimation

The equations of discrete-time Kalman filter algorithm are as follows.

The initialized state and covariance are

$$\begin{aligned} \hat{x}_0^+ &= E(x_0) \\ P_0^+ &= E[(x_0 - \hat{x}_0^+)(x_0 - \hat{x}_0^+)^T] \end{aligned} \tag{4-27}$$

The time updates equations are

$$\hat{x}_k^- = F_{k-1}\hat{x}_{k-1}^+ + G_{k-1}u_{k-1} \tag{4-28}$$

$$P_k^- = F_{k-1}P_{k-1}^+F_{k-1}^T + Q_{k-1} \tag{4-29}$$

The measurement updates equations are

$$K_k = P_k^- H_k^T (H_k P_k^- H_k^T + R_k)^{-1} = P_k^+ H_k^T R_k^{-1} \tag{4-30}$$

$$\hat{x}_k^+ = \hat{x}_k^- + K_k(y_k - H_k\hat{x}_k^-) \tag{4-31}$$

$$P_k^+ = (I - K_k H_k)^T P_k^- (I - K_k H_k) + K_k R_k K_k^T = (I - K_k H_k)^T P_k^- \tag{4-32}$$

From the above equations we can see that after the time and measurement updated at each time step, the recursive algorithm keeps using the previous posterior estimate to predict the new priori estimate. Because Kalman filter only uses the previous state to predict the current states, it is much easier and flexible to make a real-world implementation of it. From equations (4-29), (4-30) and (4-32), we found the calculation of error covariance P_k and Kalman gain K_k is not based on the measurements y_k. It only depends on the dynamic system parameters F_k and G_k and tuning noise covariance Q_k and R_k (Q_k and R_k are the tuning parameters of Kalman filter which we will discuss later). This fact makes Kalman filter more feasible, because all the error covariance and gains of Kalman filter can be calculated. The operating process of standard Kalman Filter is shown in Fig 16.

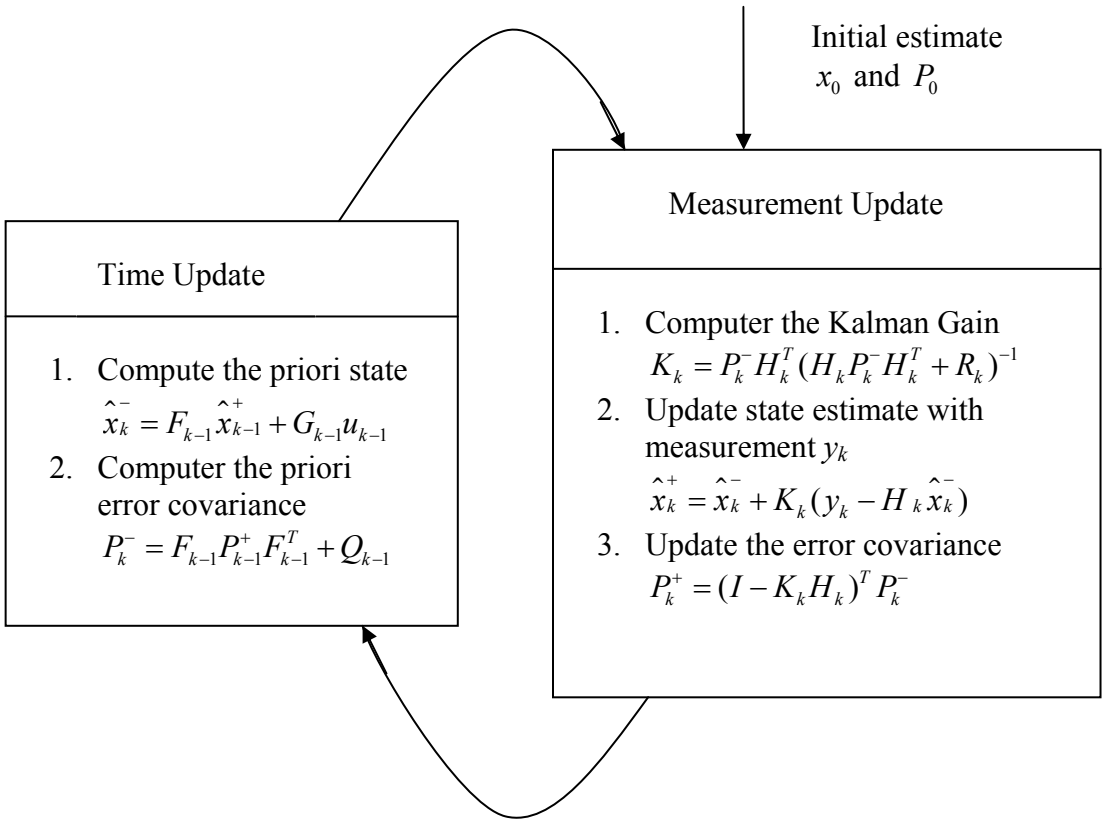

Figure 16: Standard Kalman Filter [15]

4.2.4 Tuning

Tuning is the process of optimizing the parameters of Kalman filters. To achieve a good performance for Kalman filter, tuning the process noise Q_k (or mechanical thermal noise) and the measurement noise covariance R_k (or electronic noise) are required. For the measurement noise, it is possible to determine the range of R_k by taking some sample measurements. However, Q_k is usually difficult to measure.

The process noise source normally represents the uncertainty of the dynamic system and we can not directly observe the process. That is the reason why we need observer. Choosing

an appropriate Q_k including uncertainty can make the system more reliable. But the larger the Q_k is chosen, the worse estimated model we will have.

4.2.5 Extended Kalman Filter (EFK)

The standard discrete-time Kalman filter gives the state estimation of a LTI system. In the real-world, there is almost no absolutely linear dynamic system or sensors. Therefore the EKF is introduced to estimate the states of non-linear dynamic systems. We can use Taylor series to expand the non-linear equations around a nominal point which includes the nominal control u_0, state x_0, output y_0 and noise w_0 and v_0. After linearization, we will employ Kalman filter to estimate the linearized state. Then we use this priori estimation as the new linearized nominal point on the next time step and implement Kalman filter theory again to estimate the new linearized model. This makes the EKF a recursive optimum state-observer that can be used for the state and parameter estimation of a non-linear dynamic system in real time. We can derive the discrete-time EKF algorithm as follows.

Suppose we have a non-linear discrete-time system model:

$$x_k = f_{k-1}(x_{k-1}, u_{k-1}, w_{k-1}) \tag{4-33}$$

$$y_k = h_k(x_{k,} v_k) \tag{4-34}$$

$$\begin{aligned} w_k &\sim (0, Q_k) \\ v_k &\sim (0, R_k) \end{aligned} \tag{4-35}$$

where the process noise w_{k-1} and measurement noise v_k are assumed to be zero-mean, white and uncorrelated noises. We can use Taylor series expansion on (4-33) to get Jacobian matrix F, which is the partial derivatives of function $f(.)$ with respect to state x, and Jacobian

matrix L, which is the partial derivatives of function $f(.)$ with respect to process noise w around the nominal state $x_{k-1} = \hat{x}_{k-1}^{+}$ and $w_{k-1} = 0$. Then we get:

$$\begin{aligned} x_k &= f_{k-1}(\hat{x}_{k-1}^{+}, u_{k-1}, 0) + \left.\frac{\partial f_{k-1}}{\partial x}\right|_{\hat{x}_{k-1}^{+}} (x_{k-1} - \hat{x}_{k-1}^{+}) + \left.\frac{\partial f_{k-1}}{\partial w}\right|_{\hat{x}_{k-1}^{+}} w_{k-1} \\ &= F_{k-1}x_{k-1} + [f_{k-1}(\hat{x}_{k-1}^{+}, u_{k-1}, 0) - F_{k-1}\hat{x}_{k-1}^{+}] + L_{k-1}w_{k-1} \\ &= F_{k-1}x_{k-1} + \tilde{u}_{k-1} + \tilde{w}_{k-1} \end{aligned} \tag{4-36}$$

$$\begin{aligned} F_{k-1} &= \left.\frac{\partial f_{k-1}}{\partial x}\right|_{\hat{x}_{k-1}^{+}} \\ L_{k-1} &= \left.\frac{\partial f_{k-1}}{\partial w}\right|_{\hat{x}_{k-1}^{+}} \end{aligned} \tag{4-37}$$

In (4-36), we defined the $f_{k-1}(\hat{x}_{k-1}^{+}, u_{k-1}, 0) - F_{k-1}\hat{x}_{k-1}^{+}$ as known control signal $\tilde{u}_{k-1}$ and $L_{k-1}w_{k-1}$ as the noise signal $\tilde{w}_{k-1}$. We can do the same thing on measurement equation (4-34) to get Jacobian matrices H and M which are the partial derivatives of function $h(.)$ with respect to x and v around the nominal point $x_k = \hat{x}_k^{-}$ and $v_k = 0$. Then we get:

$$\begin{aligned} y_k &= h_k(\hat{x}_k^{-}, 0) + (x_k - \hat{x}_k^{-}) + \left.\frac{\partial h_k}{\partial v}\right|_{\hat{x}_k^{-}} v_k \\ &= H_k x_k + [h_k(\hat{x}_k^{-}, 0) - H_k\hat{x}_k^{-}] + M_k v_k \\ &= H_k x_k + z_k + \tilde{v}_k \end{aligned} \tag{4-38}$$

$$\begin{aligned} H_k &= \left.\frac{\partial h_k}{\partial x}\right|_{\hat{x}_k^{-}} \\ M_k &= \left.\frac{\partial h_k}{\partial v}\right|_{\hat{x}_k^{-}} \end{aligned} \tag{4-39}$$

In (4-38), the measurement equation is defined based on the known signal $z_k = h_k(\hat{x}_k^{-}, 0) - H_k\hat{x}_k^{-}$ and measurement noise $\tilde{v}_k = M_k v_k$. Combining (4-36) with (4-38), we

get a linear dynamic system at each time step. Standard discrete-time Kalman filter algorithm can be applied to estimate the state. The equations of discrete-time Kalman filter algorithm are as follows.

The initialized state and covariance:

$$\begin{aligned} \hat{x}_0^+ &= E(x_0) \\ P_0^+ &= E[(x_0 - \hat{x}_0^+)(x_0 - \hat{x}_0^+)^T] \end{aligned} \tag{4-40}$$

Computing the partial derivative matrices of dynamic equation yields

$$\begin{aligned} F_{k-1} &= \left.\frac{\partial f_{k-1}}{\partial x}\right|_{\hat{x}_{k-1}^+} \\ L_{k-1} &= \left.\frac{\partial f_{k-1}}{\partial w}\right|_{\hat{x}_{k-1}^+} \end{aligned} \tag{4-41}$$

The time-update equations are given by

$$P_k^- = F_{k-1} P_{k-1}^+ F_{k-1}^T + L_{k-1} Q_{k-1} L_{k-1}^T \tag{4-42}$$

$$\hat{x}_k^- = f_{k-1}(\hat{x}_{k-1}^+, u_{k-1}, 0) \tag{4-43}$$

Computing the partial derivative matrices of measurement equation gives

$$\begin{aligned} H_k &= \left.\frac{\partial h_k}{\partial x}\right|_{\hat{x}_k^-} \\ M_k &= \left.\frac{\partial h_k}{\partial v}\right|_{\hat{x}_k^-} \end{aligned} \tag{4-44}$$

Measurement-update equations are

$$K_k = P_k^- H_k^T (H_k P_k^- H_k^T + M_k R_k M_k^T)^{-1} \tag{4-45}$$

$$\hat{x}_k^+ = \hat{x}_k^- + K_k[y_k - h_k(\hat{x}_k^-, 0)] \tag{4-46}$$

$$P_k^+ = (I - K_k H_k) P_k^- \tag{4-47}$$

The EKF algorithms are implemented on nonlinear dynamics and are used to estimate the states for nonlinear systems. The calculation of error covariance matrices are dependent upon consistent linearization which are based upon most recent state estimates. System Jacobian matrices F and measurement Jacobians H are time varying matrices. Their values are based on the most recent state estimates. Also the priori estimate error covariance P_k^-, the posteriori estimate error covariance P_k^+ and the Kalman gain K_k are time varying matrices based on the most recent state estimates. The EKF needs to be calculated online. The calculation for EFK is more complicated than the one for standard Kalman filter. When EKF is applied to real-system, a fast digital computational device has to be used for the online matrix computation.

4.2.6 Hybrid Extended Kalman Filter

For most real engineering problems, systems are working as continuous time dynamic processes but the measurements are obtained by discrete-time samplings. In this section, a hybrid EKF based on the continuous-time dynamic system and discrete-time measurements is introduced. Its implementation becomes more and more popular in today's digitalized world.

The differences between discrete-time EKF and hybrid EKF are the time update equations and discrete model. Suppose we have hybrid system equations as follows:

$$\begin{aligned} \dot{x}(t) &= Ax(t) + Bu(t) + Lw(t) \\ y_{(k)} &= H_{(k)}x_{(k)} + v_{(k)} \end{aligned} \tag{4-48}$$

$$\begin{aligned} w(t) &\sim (0, Q) \\ v_k &\sim (0, R_k) \end{aligned} \tag{4-49}$$

Comparing (4-48) and (4-49) with the discrete-time equations (4-23) and (4-24), we can see the differences between discrete-time EFK and hybrid EFK are A, B and $F_{(k)}$, $G_{(k)}$. As shown it (4-25), $F_{(k)}$ and $G_{(k)}$ are discretized from continuous dynamic system matrices A and B. Same as the discrete-time EKF, we use priori estimation state as the linearization nominal point to obtain the continuous-time system for time update equations. The equations of hybrid EKF algorithm are given as follows.

The initialized state and covariance are given by

$$\begin{aligned} \hat{x}_0^+ &= E(x_0) \\ P_0^+ &= E[(x_0 - \hat{x}_0^+)(x_0 - \hat{x}_0^+)^T] \end{aligned} \tag{4-50}$$

Computing the partial derivative matrices of dynamic equation produces

$$\begin{aligned} A &= \left.\frac{\partial A}{\partial x}\right|_{\hat{x}_{k-1}^+} \\ L &= \left.\frac{\partial L}{\partial w}\right|_{\hat{x}_{k-1}^+} \end{aligned} \tag{4-51}$$

The times update equations are

$$\dot{P} = AP + PA^T + LQL^T \tag{4-52}$$

$$\dot{\hat{x}} = A\hat{x}(t) + Bu(t) \tag{4-53}$$

We start this update with $\hat{x}(t) = \hat{x}_{k-1}^+$ and $P = P_{k-1}^+$. After integration we get $\hat{x}_k^- = \hat{x}$ and $P_k^- = P$.

Computing the partial derivative matrices of measurement equation yields

$$H_k = \left.\frac{\partial h_k}{\partial x}\right|_{\hat{x}_k^-}$$
$$M_k = \left.\frac{\partial h_k}{\partial v}\right|_{\hat{x}_k^-} \tag{4-54}$$

Measurement-update equations are

$$K_k = P_k^- H_k^T (H_k P_k^- H_k^T + M_k R_k M_k^T)^{-1} \tag{4-55}$$

$$\hat{x}_k^+ = \hat{x}_k^- + K_k[y_k - h_k(\hat{x}_k^-, 0)] \tag{4-56}$$

$$P_k^+ = (I - K_k H_k) P_k^- \tag{4-57}$$

The block diagram for hybrid Kalman filter observer is shown in Fig. 17. The continuous block in Fig 7 is the system working in continuous. The measurement update block represents the discrete-time measurement-update equations. The time update block represents the continuous time-update equations.

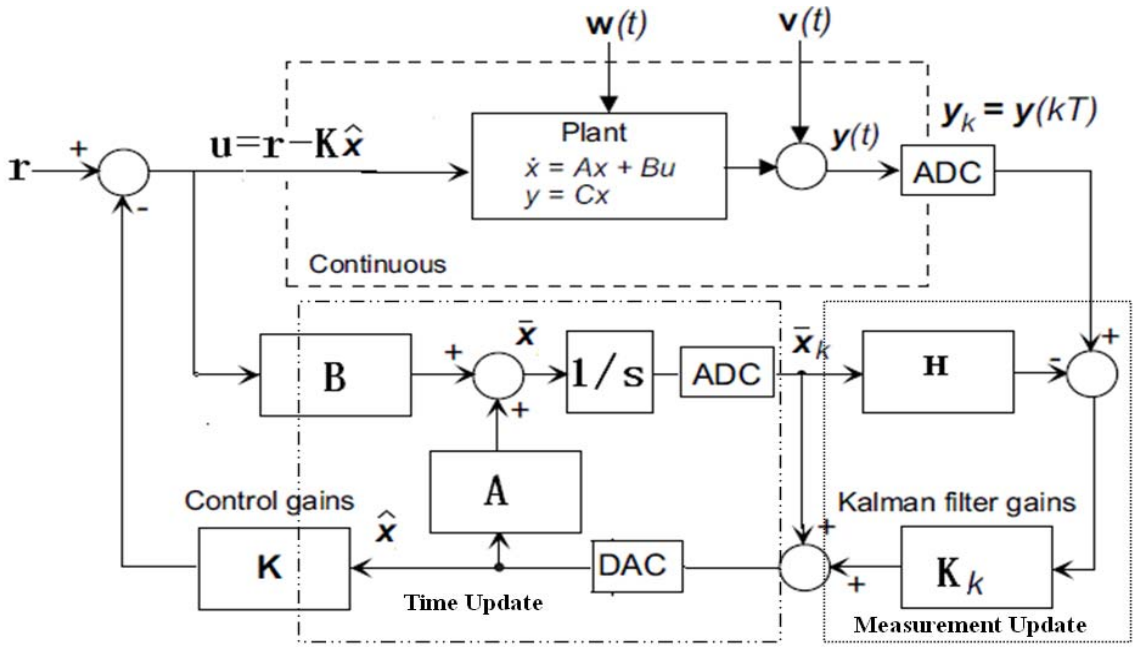

Figure 17: Closed-loop control with hybrid EKF based observer

4.3 Summary of this chapter

In this section, we started with investigating what state observer is. Then we discussed the basic Luenberger observer to get a brief review about how an observer works. Then we took a close look at the Kalman filter through discussing the conditions under which it works as an optimal estimator. The properties of Kalman filter were proved. The discrete time Kalman filter which is normally used in LTI system is shown in this chapter. The parameters of Kalman filter are calculated. Tuning of the Kalman filter is discussed to achieve a good performance of it. We also discussed the application of EKF on non-linear dynamic systems in real world. But the EFK need more calculations that require much faster computational device. Finally hybrid EKF which is the most practical observer in real engineering system is introduced. The hybrid EFK will be used in MEMS accelerometer system.

CHAPTER V

SIMULATION RESULTS AND STABILITY ANALYSIS

In this chapter, we will conduct the simulation of the hybrid EFK on a MEMS accelerometer model. Two goals have to be achieved by the hybrid EFK. They are obtaining an estimated acceleration with reduced noise floor and high SNR, and improving the accelerometer system's performance in stability, linearity, and dynamic operating range. Two sets of simulation results will be shown in this chapter. The first set of simulation results is to test the effects of noise on three different systems, which are open-loop system, force-to-rebalance closed-loop system, and Kalman filter observed closed-loop system. Three different sinusoidal acceleration signals are used for the first set of simulation. The second set of simulation results is based on the Kalman-filter-observed closed-loop system. In the second set of simulations, we choose different percentage values of the process noise covariance and measurement noise covariance to test the tuning performance of hybrid EKF with uncertain noise consideration. All the simulations in this thesis are completed in MATLAB/Simulink®.

5.1 MEMS accelerometer with hybrid EKF model and stability analysis

In the following simulations, we chose sinusoidal acceleration input at the frequency of $10\ Hz$, and with $500ug$ thermal-mechanical Brownian noise. Also we chose $1MHz$ as readout circuit's operation frequency, and chose a big electronic noise at $0.02g$. For a MEMS accelerometer which has sensitivity about $1\ mV/g$, the electronic noise is much more significant than thermal-mechanical noise.

We will use the hybrid EKF state equation (4-48) to estimate the acceleration signal for MEMS accelerometers. The matrices *A, B* and *H* are given in (5-1), (5-2) and (5-3). The mechanical and electronic parameters for the accelerometer are given in Table 1. In addition, the parameters which are used in hybrid EKF state equations are shown in Table 2. Whether the accelerometer system is linear or non-linear depends on the damping coefficient *b* we choose.

$$A = \begin{bmatrix} 0 & 1 \\ -k/m & -b/m \end{bmatrix} \tag{5-1}$$

$$B = L = \begin{bmatrix} 0 \\ 1/m \end{bmatrix} \tag{5-2}$$

$$H = \begin{bmatrix} \frac{2\varepsilon_0 \varepsilon_r AV1}{C_4 d_0^2} & 0 \end{bmatrix} \tag{5-3}$$

Table II: Addition system parameters

Brown noise (Process noise) $F_B = Q$	$3.35e-23N$
Electrical noise (Measurement noise) $V_N = R_k$	4.88e-8 V
Initial state $x0$	[0;0]
Initial covariance of estimation error P	[0 0;0 0]
Sinusoid input frequency w	20π

To satisfy the requirements for Kalman filter which we discuss in chapter 4, we need check the stability of A, and observability of (A H).

$$eigen(A) = 1.0e+005 * \begin{bmatrix} -0.0439 \\ -1.7982 \end{bmatrix} \tag{5-4}$$

$$rank(O) = rand(\begin{bmatrix} H \\ HA \end{bmatrix}) = 2 \tag{5-5}$$

In (5-5), matrix O is observation matrix which is used to check the observability of the system. From (5-4), we can see that all of the eigenvalues of state matrix A have negative real parts. So according to Lyapunov's indirect method, the system is asymptotically stable. From (5-5), O is a full-rank matrix. So the system is also observable. Also we assume the process noise and measurement noise are independent white noise. Now we can construct the hybrid EKF on MEMS accelerometer model to get the properties of Kalman filter which are obtained in equations (4-9) and (4-10).

5.2 Open-loop, force-to-rebalance closed-loop and hybrid EKF observer based closed-loop MEMS accelerometer systems

In this set of simulations, we are going to test the performance of three different MEMS accelerometer system configurations. The first configuration is open-loop system which is shown in Fig 14. The second configuration is force-to-rebalance closed-loop system which is shown in Fig 13. The third configuration is hybrid EKF observer based closed-loop system which is shown in Fig 17. The mechanical and electronic parameters are given in Table 1. We can obtain the Brownian and electronic noises from equations (3-2) and (3-10) and use them as process noise covariance Q and measurement noise covariance R of hybrid EKF.

In Chapter 2, we discussed the advantages of closed-loop MEMS accelerometer system over the open-loop system. The major advantage of closed-loop system is its negative feedback that leads to stability, wide dynamic range, and good linearity of the accelerometer system. In chapter 3, the noise consideration tells us the SNR of closed-loop system is lower than that of the open-loop. That means small input of a closed-loop system can result in a lot more noisy output and makes it harder to determine small acceleration. In chapter 4, we introduce the hybrid EKF observer to the MEMS accelerometer system to not only keep the advantage of the closed-loop configuration, but also obtain the good SNR performance. In order to test the effectiveness of hybrid EFK, we are going to use different input accelerations from $0.1\,g$ to $10\,g$ to monitor the accelerometer's outputs and seismic mass' displacements.

Fig. 18, Fig. 19, and Fig. 20 show the voltage and displacement outputs of MEMS accelerometer in an open-loop configuration as the input acceleration's magnitude are 0.1*g*, 1*g*, and 5*g*.

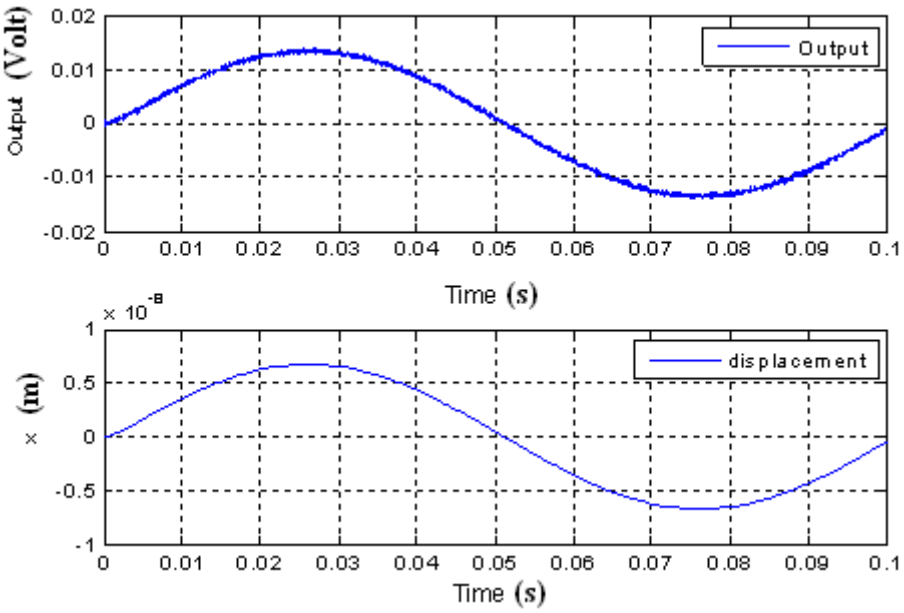

Figure 18: Open-loop system with 0.1g sinusoid input

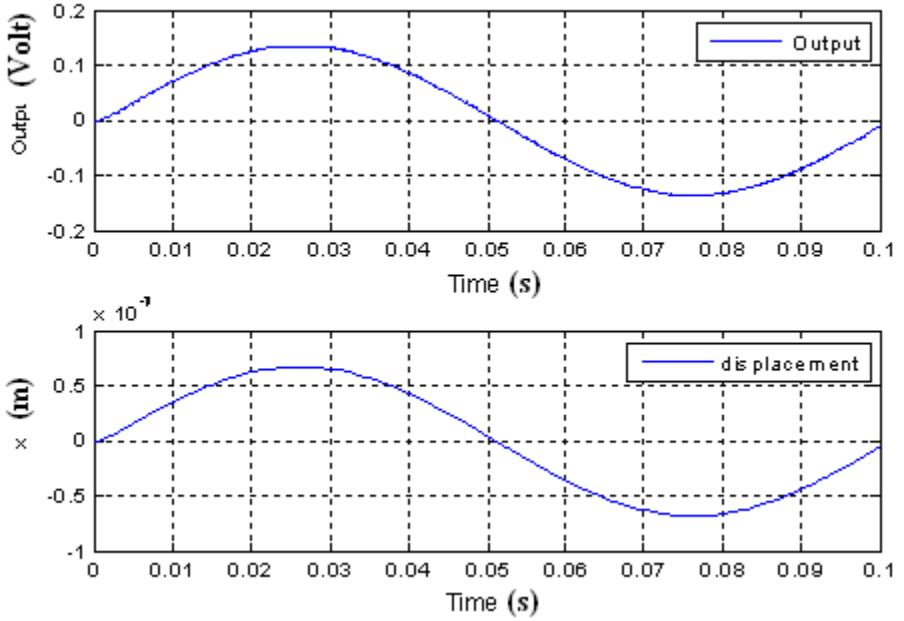

Figure 19: Open-loop system with 1g sinusoid input

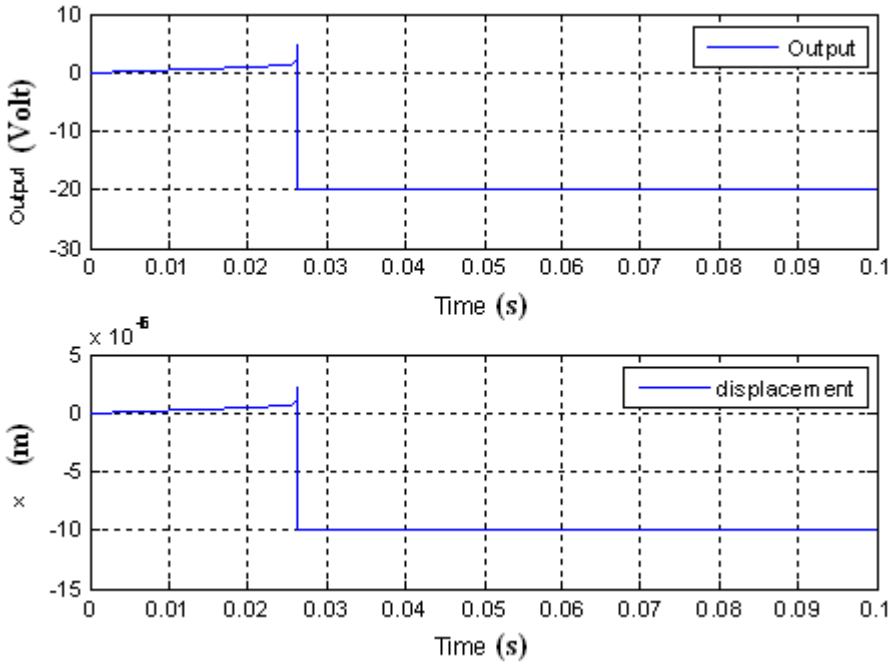

Figure 20: Open-loop system with 5g sinusoid input

The simulation results about force re-balanced closed-loop MEMS accelerometer system are shown in Fig. 21, Fig. 22, and Fig. 23.

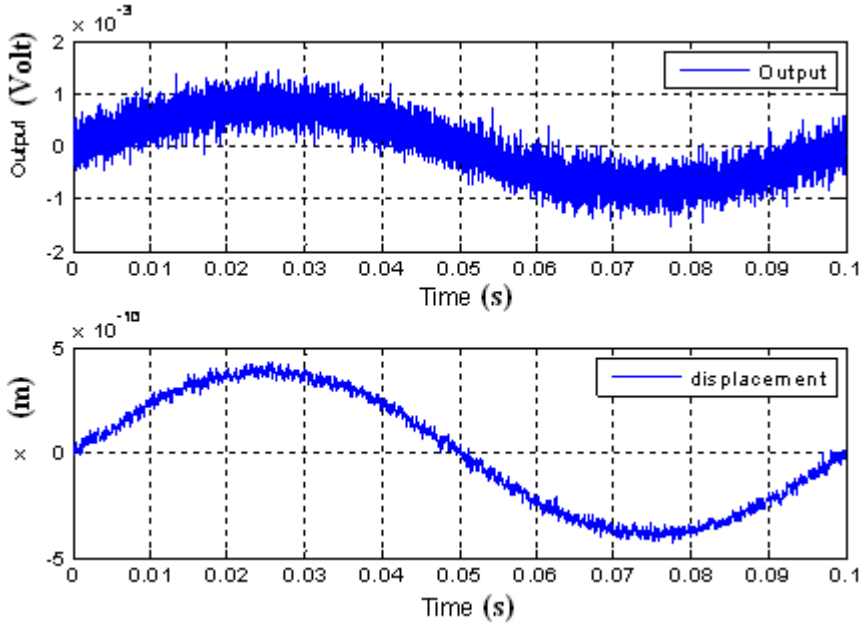

Figure 21: Closed-loop system with 0.1g sinusoid input

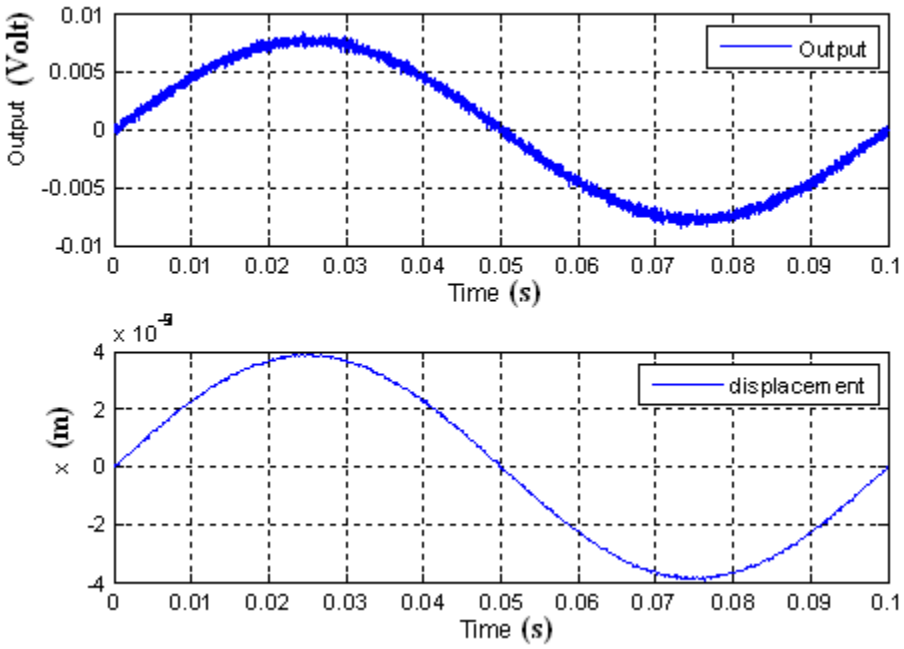

Figure 22: Closed-loop system with 1g sinusoid input

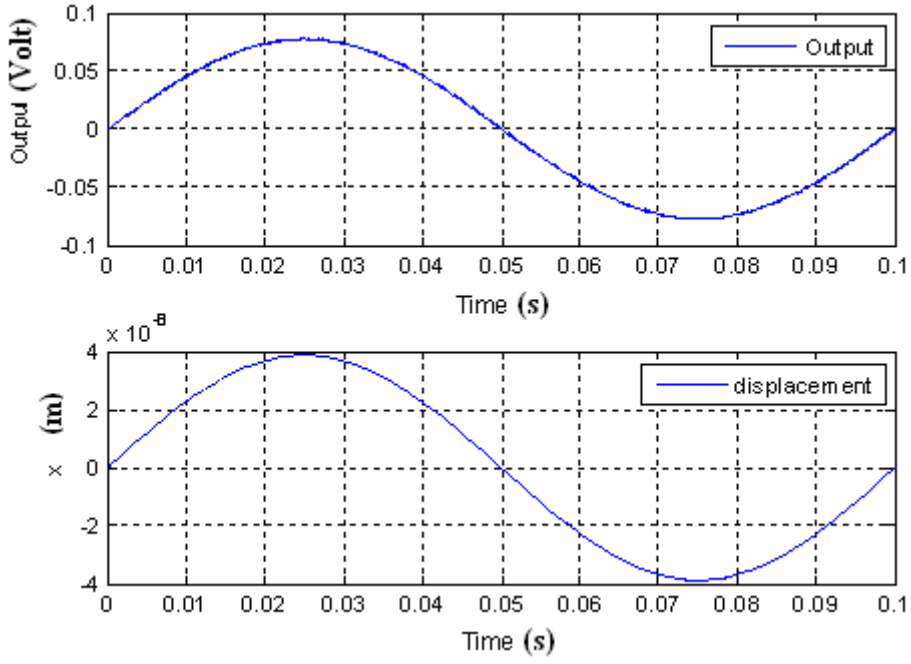

Figure 23: Closed-loop system with 1g sinusoid input

The simulation results about hybrid EKF observer based closed-loop MEMS accelerometer system are shown in Fig. 24, Fig. 25, and Fig. 26. These three results show the estimated output always has better SNR than real output.

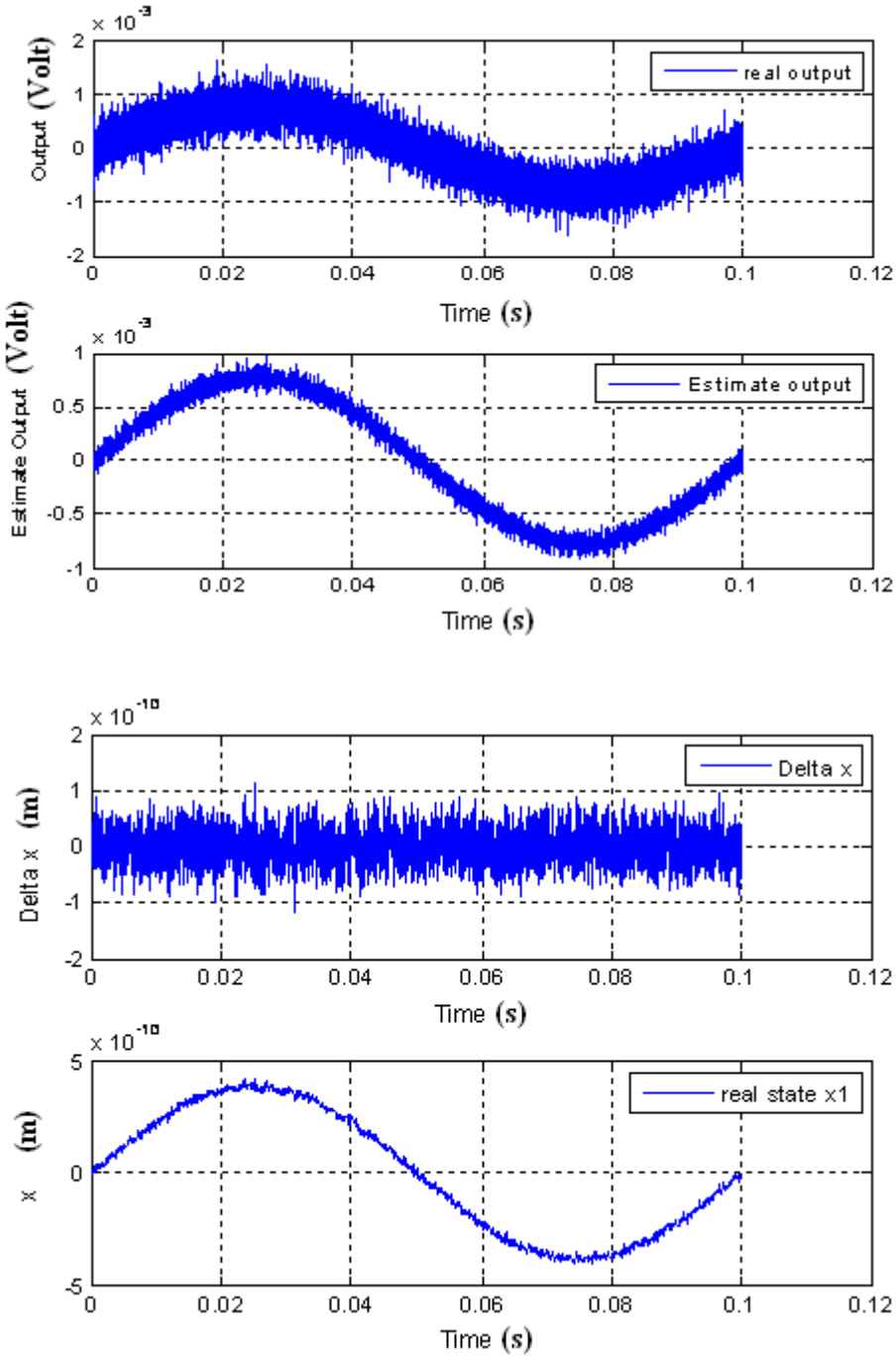

Figure 24: Hybrid EKF observer closed-loop system with 0.1g sinusoid input

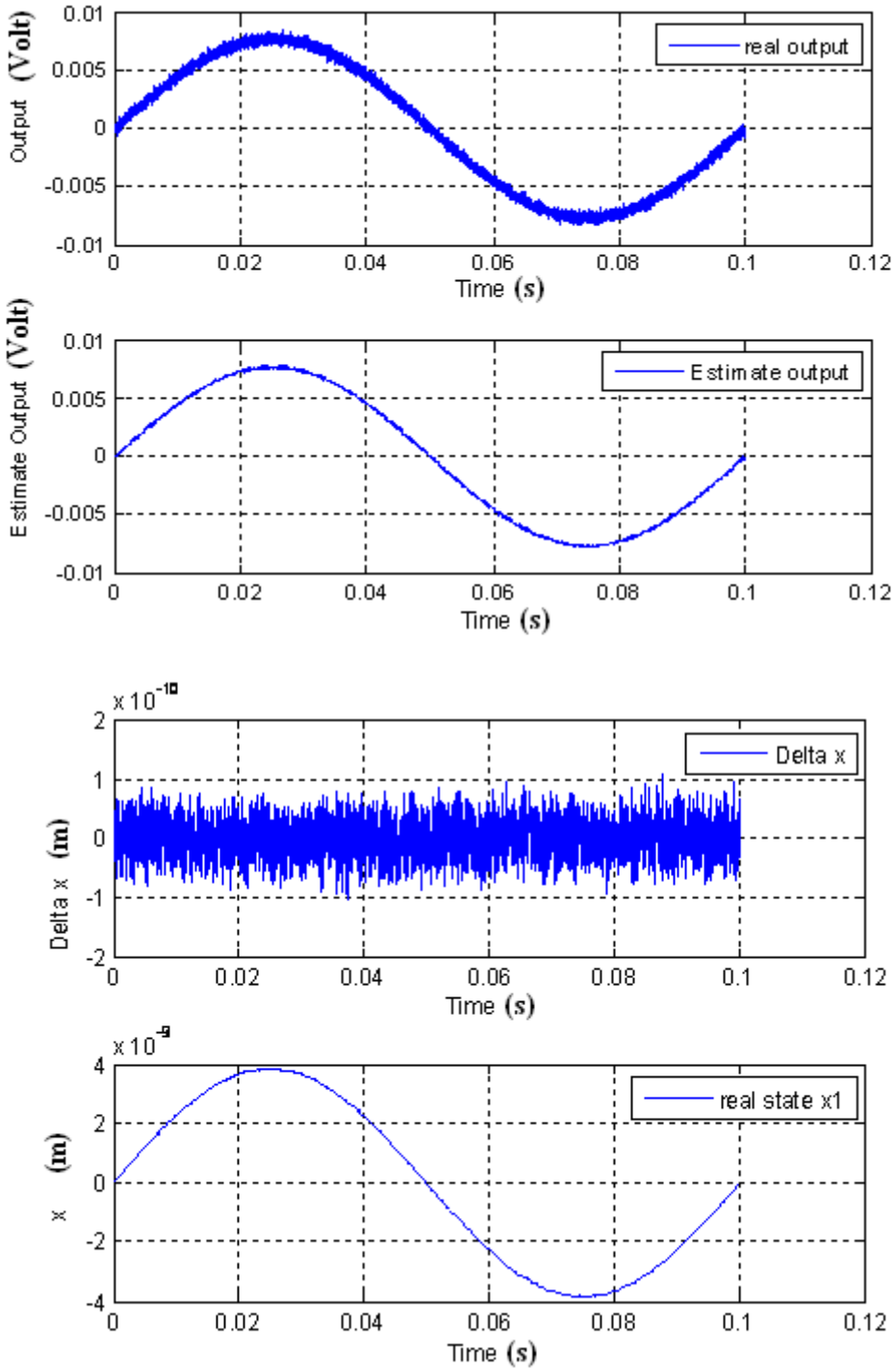

Figure 25: Hybrid EKF observer closed-loop system with 1g sinusoid input

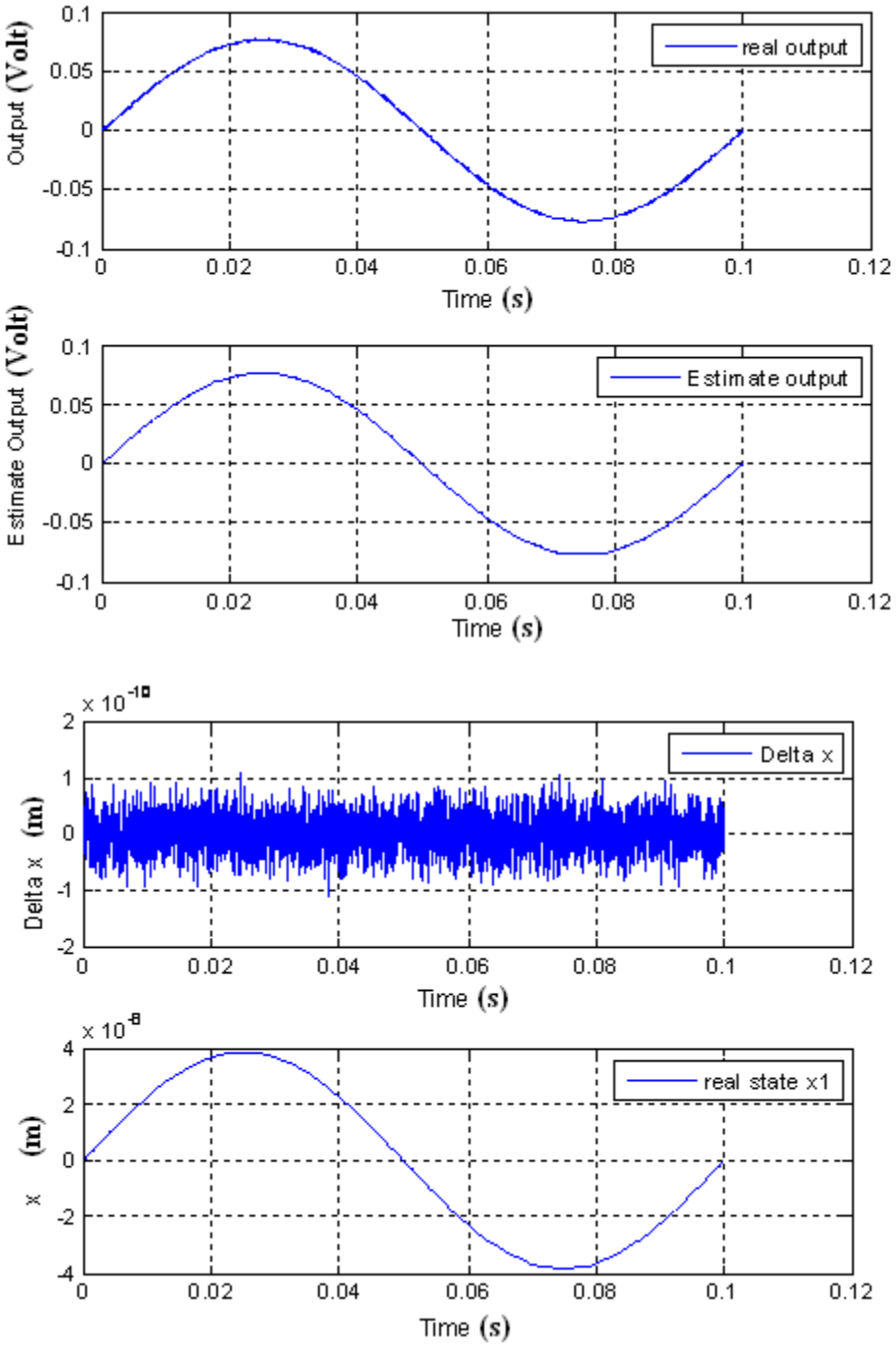

Figure 26: Hybrid EKF observer closed-loop system with 10g sinusoid input

A brief summary of the simulation results listed above is given in Table 3. Table 3 shows the different SNRs and mass' maximum displacements for open-loop system, force-to-rebalance closed-loop control system, and hybrid observer based closed-loop system respectively.

Table III: Comparison of three different MEMS accelerometer systems

Input acceleration's magnitude	Open-loop		Force re-balanced closed-loop		Hybrid EKF observer closed-loop	
	Output SNR	Mass max displacement	Output SNR	Mass max displacement	Output SNR	Mass max displacement
$0.1\,g$	>40 dB	$7.00e-09$ m	4 dB	$4.00e-10$ m	12 dB	$4.00e-10$ m
$1\,g$	>40 dB	$7.00e-08$ m	24 dB	$4.00e-9$ m	32 dB	$4.00e-9$ m
$5\,g$	unstable	exceed limit				
$10\,g$	N/A	N/A	>40 dB	$4.00e-8$ m	>40 dB	$4.00e-8$ m

Open-loop structure has a dynamic range up to $5\,g$. The positive feedback in the open-loop system makes it unstable. Therefore the accelerator under open-loop control can not track the acceleration input with a magnitude larger than 5*g*. Also, larger mass' displacement in open-loop system makes the accelerometer more non-linear, and makes the mass' displacement close to the capacitive parallel plate's pull-in distance between fixed plate and movable seismic mass. As the pull-in phenomenon occurs, the movable mass will be pulled to either bottom or top plate, causing the failure of operation. Force-to-rebalanced closed-loop structure increases the dynamic range of accelerometers and can track up to $10\,g$ acceleration. The negative feedback in closed-loop system gives a smaller mass' displacement and produces a more linear system compared to open-loop system. But because of the noisy feedback, the smaller SNR in force-to-rebalance system makes it difficult to identify small acceleration inputs. Hybrid EKF observer based closed-loop structure keeps the advantage of closed-loop systems with wide dynamic range and small mass displacement.

Hybrid EKF observer based closed-loop system also has a better SNR than the one for force-to-rebalanced closed-loop structure. In the Hybrid EKF simulation, $\tilde{x}$ which is the difference between the estimated displacement $\hat{x}$ and real displacement x, has a zero mean and $1.00e-10m$ covariance error no matter what the magnitude of input acceleration is. We can also get better SNR with the hybrid EKF observer.

The simulation results verified the effectiveness of the hybrid EFK. We also demonstrated in our simulation results that the hybrid EKF observer can improve the performance of MEMS accelerometer system. In next section, we will conduct more simulations on hybrid EKF to observe the system's tuning performance and of its robustness against system uncertainties.

5.3 Hybrid EKF MEMS accelerometer tuning and uncertain parameter analysis

All the simulation results of hybrid EKF in section V.1 are based on the accurate model of a MEMS accelerometer system. In the real world, it is impossible to obtain a perfect model of real system, especially the exact values of system parameters. As we discussed in chapter 2, MEMS accelerometers have a very simple mass-damper-spring structure, but still have uncertain parameters such as mass, damping coefficient and spring constant. Particularly in MEMS system, we can not measure these system parameters directly and all the parameter values are from calculations. These uncertain parameters can affect state matrix A and give a total different system model which is difficult to be estimated by Kalman filter. Alternative methods should be introduced to the accelerometer system such as adaptive law, linear quadratic regulator and multiple-model estimation and so on which we

are not going to discuss here. However, the Brownian noise and electronic noise can be estimated, and they are the uncertainty that the Kalman filter can deal with. If we consider the system as a linear system, the process noise covariance Q and the measurement noise covariance R can be pre-computed to get the Kalman gain K_k and estimation covariance P for the design of Kalman filter.

In the simulation of this section, we will tune the Q and R and obtain the estimated output, state estimation error, and standard deviation (STD) for state estimation error. We will investigate how Q and R affect the measurement of MEMS accelerometers. This system model is a linear system for which we use the small-deflection damping coefficient. The MEMS accelerometer's parameters are given in Tables 1 and 2 and the sinusoidal input acceleration is $0.1\,g$.

The simulation results about the hybrid KF observer based closed-loop system with different Q and R are shown in figures from 27 through 31.

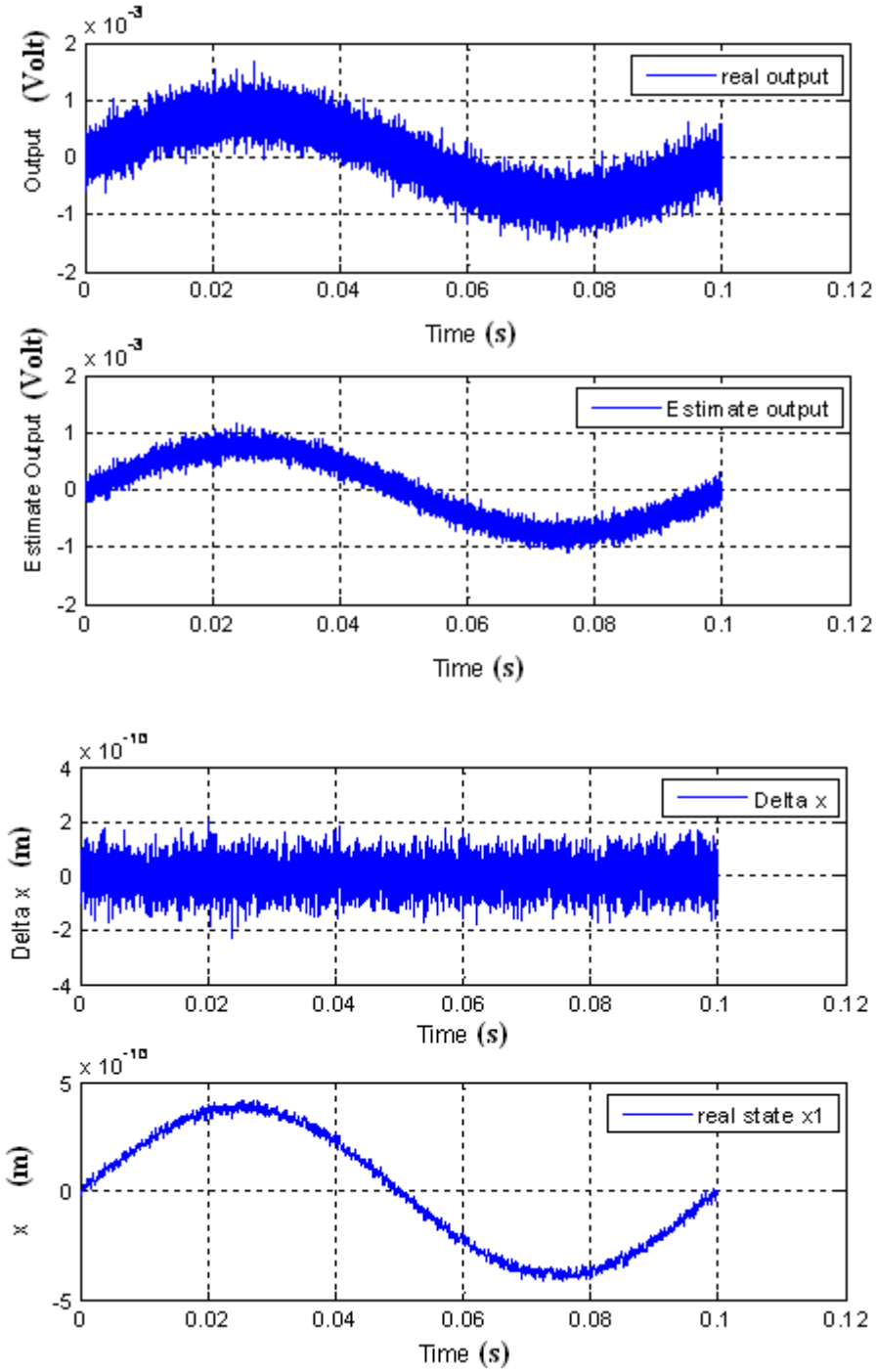

Figure 27: Estimated and actual outputs of hybrid KF observer based closed-loop system with increased Q by ten times

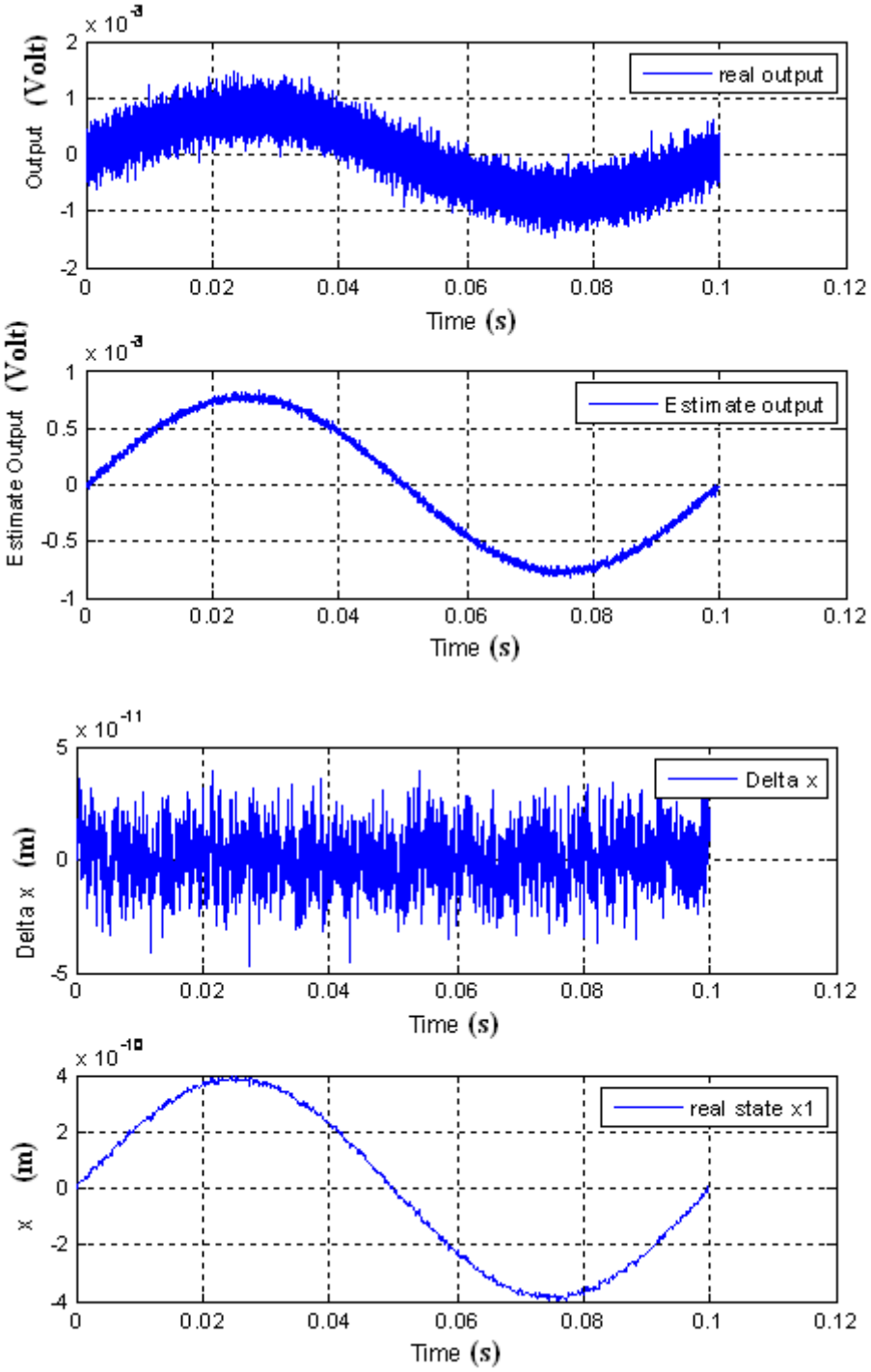

Figure 28: Estimated and actual outputs of hybrid KF observer based closed-loop system with reduced Q by ten times

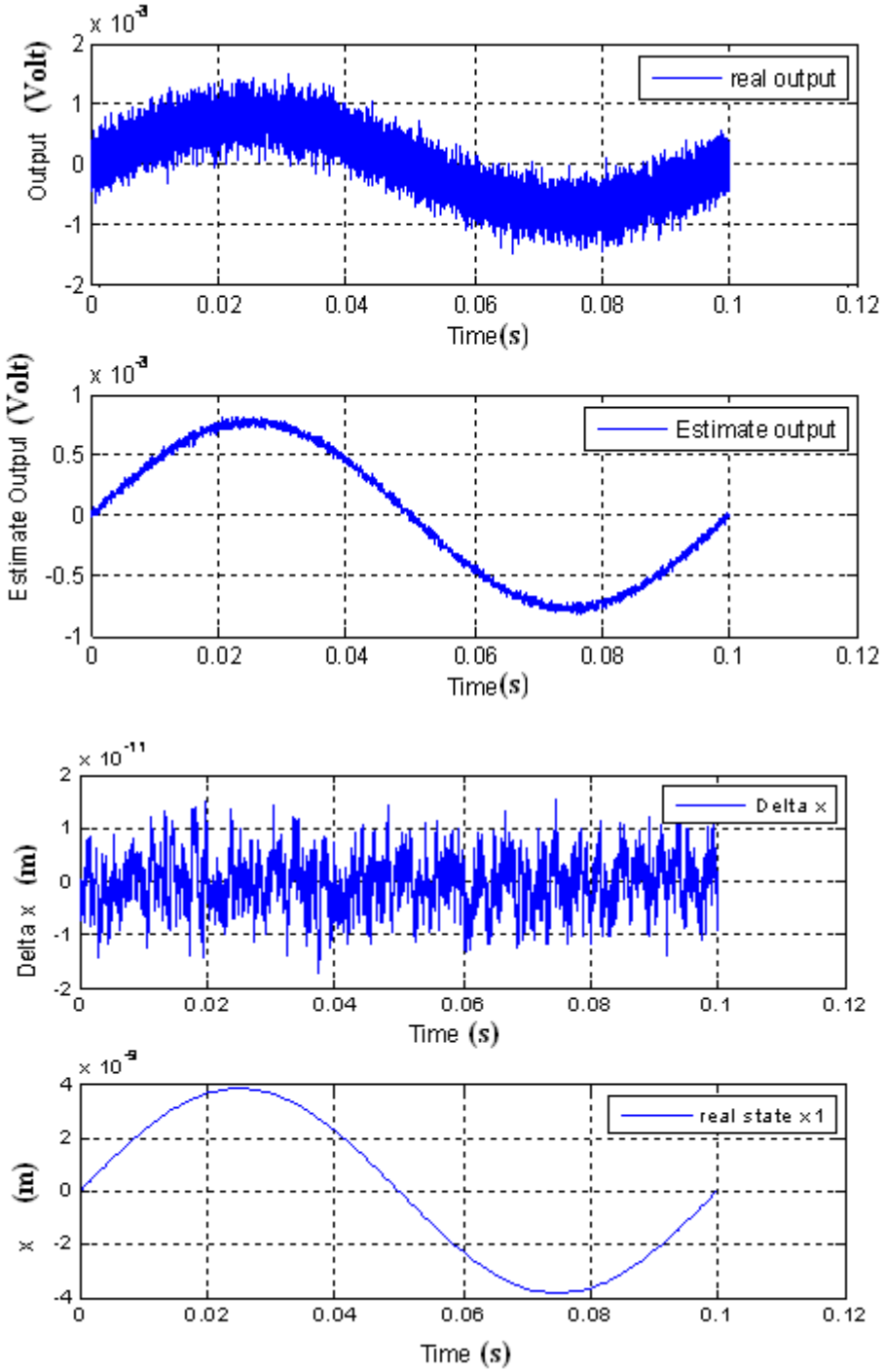

Figure 29: Estimated and actual outputs of hybrid KF observer based closed-loop system with increased *R* by ten times

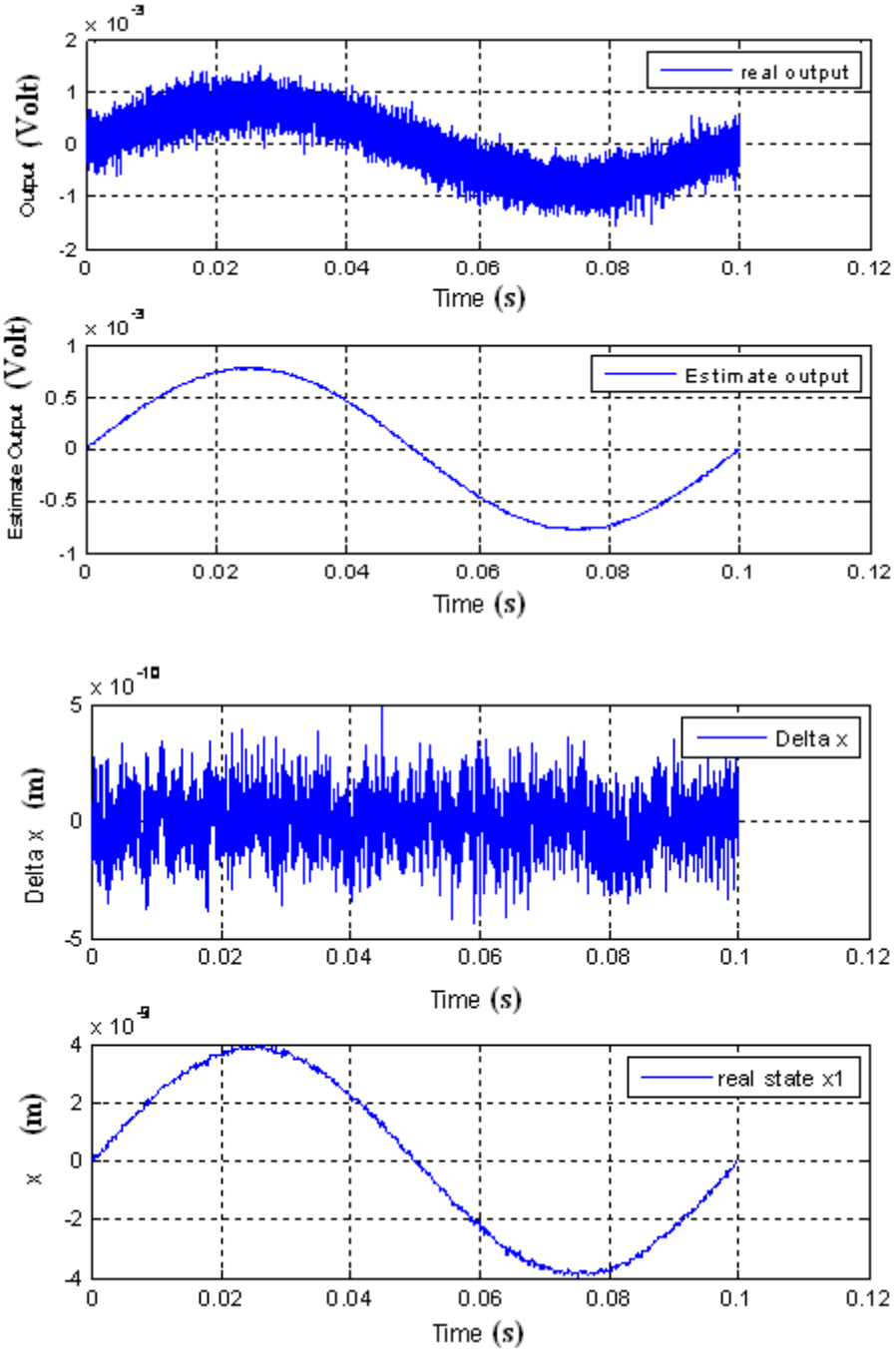

Figure 30**:** Estimated and actual outputs of hybrid KF observer based closed-loop system with reduced *R* by ten times

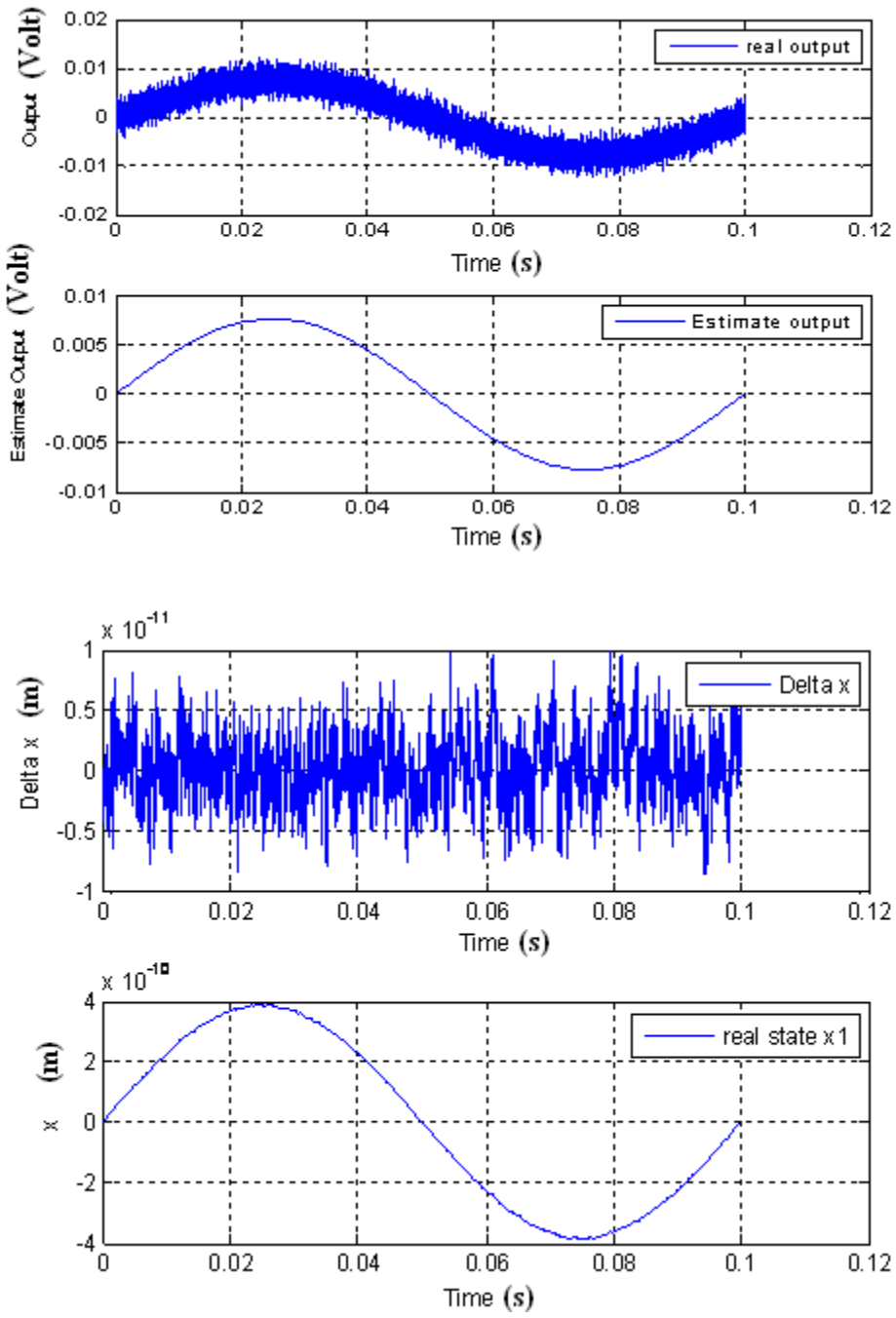

Figure 31: Estimated and actual outputs of hybrid KF observer based closed-loop system with reduced *R* by ten times

From the figures above, we can see that decreasing Q and increasing R can improve the noise performance on estimated output. The reason is because the electronic noise is hundreds times bigger than thermal-mechanical Brownian noise. Increasing the power of measurement noise covariance R gives a better performance of the Kalman filter. The best performance we get is when we choose increased R by 10 times reduced Q by 10 times. If we decrease Q and increase R by more than 10 times, the performance will not become better and will remain unchanged. Also, decreasing Q and increasing R too much will make the estimation covariance P not semi-positive, which can ruin the Kalman filter and make it total not workable.

The output SNRs, maximum estimation errors, and the STDs of estimation errors for different process noise covariance Q and measurement noise covariance R are shown in the Table IV.

Table IV: Different SNRs, maximum estimation errors, and STDs with different Q and R

	Output SNR	Max estimation error	STD of estimation error
Exact Q, R	12 dB	4.00e-10	2.8023e-011
Increased Q by 10 times	10 dB	2.00e-10	5.1756e-011
Reduced Q by 10 times	24 dB	4.50e-11	1.1336e-011
Increased R by 10 times	24 dB	1.50e-11	1.1943e-011
Reduced R by 10 times	10 dB	5.00e-10	5.2502e-011
Increased R by 10 times and reduced Q by 10 times	>40dB	1.00e-11	2.7512e-012

5.4 Summary of this chapter

In this chapter, we constructed a hybrid EKF on a MEMS accelerometer model and analyzed the stability of the Kalman filter observed closed-loop system. Then we simulated the observer system, investigated the system performances of open-loop system, force rebalance closed-loop system, and hybrid EKF observer based closed-loop system. At last we discussed the tuning of Kalman filter. These simulation results verified the effectiveness of the hybrid EKF in noise rejection.

CHAPTER VI

CONCLUSION AND FUTURE WORK

6.1 Conclusion

This thesis introduced a hybrid EKF with force-to-rebalance feedback control to increase MEMS accelerometers' SNR. The major noise sources, which are mechanical thermal and electronic noises, have been modeled and discussed. The properties of Kalman filter have been explained in detail and the algorithm of hybrid EKF has been developed. MEMS accelerometer was modeled and simulated on three different system configurations that are open-loop, force-to-rebalance closed-loop, and hybrid extended Kalman filter based closed-loop systems. The simulation results verified the effectiveness of hybrid EKF which not only improves the SNR of MEMS accelerometer system but keep the advantages of force-to-rebalance feedback control. In addition, tuning the process noise covariance and measurement noise covariance are discussed. The tuning process can be against uncertain parameters and hence improve the performance of hybrid EKF.

6.2 Future work

In the future, the following research on both hybrid EKF and MEMS accelerometer is expected to be conducted.

Because a hybrid EKF is mainly discrete-time, digitalizing the observer based MEMS accelerometer model is highly expected for the implementation of the hybrid EFK. In order to digitalize the currently continuous-time LTI system, the sampling time of digitalization should be chosen smaller than the inverse of maximum eigenvalue ($\frac{1}{\max\|\lambda_i\|}$) of state matrix A . For the accelerometer used in this thesis, the sampling time is smaller than $5\mu s$. It means all of the calculations for hybrid EKF should be completed within $5\mu s$. The small sampling time ($5\mu s$) proposed a big challenge of implementing the hybrid EFK using embedded system which has to follow fast-changing control signals. In the future, the author plans to investigate the feasibility of implementing the hybrid EFK using digital systems and eventually to implement the observer with hardware.

As we discussed in chapter 3, measurement noise is much bigger than process noise in MEMS accelerometer. An alternative least squares estimation method, which focuses on the estimation of measurement noise, will be added to the Kalman filter. This alternative method with less calculation could give us more practical result for the accelerometer's noise rejection. The development of such a least square estimation method will be our future work on MEMS accelerometer.

As we discussed in chapter 5, the Kalman filter works well with accurate system model and noise statistics. The filter estimates will be degraded if the system model is not accurate in the real world. For the noise covariance uncertainty and uncertainty brought by the non-

linear system, tuning the EKF would help. But for the problem with uncertainties in the stateer matrix A and the measurement matrix C, tuning EFK will not solve the problem. Therefore, in the future, we need to develop a robust Kalman filter to make it robust against system uncertainties.

REFERENCES

[1] Tai-Ran. Hsu, *MEMS & Microsystems: Design, Manufacture, and Nanoscale Engineering*, WILEY INTERSCIENCE, 2008.

[2] J. Bernstein, "Low-Noise MEMS Vibration Sensor for Geophysical Application," *Journal of Microeceltromechanical System*, vol.8, no. 4, pp. 433-438, 1999.

[3] G. Zhang, "Design and Simulation of a COMS-MEMS Accelerometer," M. S. Thesis, Department of Electrical and Computer Engineering, Carnegie Mellon University, 1998.

[4] J. Doscher, "Using iMEMS Accelerometers in Instrument Applications," Analog Devices Technical Note, available at *http://www.analog.com/industry/iMEMS/Library/*.

[5] G.K. Fedder, "Simulation of Microelectromechanical System," Doctoral Dissertation, Department of Electrical Engineering and Computer Sciences, University of California at Berkeley, 1997.

[6] T.Smith, "A 15b Electromechanical Sigma-Delta Converter for Acceleration Measurements," in *Proc. of IEEE Int. Solid-State Circuits Conf. Digest of Technical Papers*, pp. 160-161, San Francisco, CA, 1994.

[7] K. H. Chau, S. Lewis, Y. Zhao, etc, "An Integrated Force-Balanced Capacitive Accelerometer for Low-G Applications," in *Proc. 8th Int. Conf. Solid-State Sensors and Actuators, and Eurosensors IX*, pp. 593-596, Stockholm, Sweden, June, 1995.

[8] N. Yazdi, K. Najafi, "An Interface IC for A Capacitive μg Accelerometer," in *Proc. of IEEE Int. Solid-State Circuit Conf. Digest of Technical Papers*, pp. 274-275, San Francisco, CA, 1999.

[9] C. Lu, M. Lemkin, B. Boser, "A Monolithic Surface Micromachined Accelerometer with Digital Output," in *Proc. of IEEE Solid-state Circuit Conf. Digest of Technical Papers*, pp.160-161, San Francisco, CA, 1995.

[10] Kraft. M, "Closed-loop Digital Accelerometer employing oversampling conversion," *Ph.D. Dissertation*, Coventry University, School of Engineering, UK, 1997.

[11] G. Zhang, "Sensing and Control Electronics for Low-Mass Low-Capacitance MEMS Accelerometer," *Ph.D. Dissertation*, Carnegie Mellon University, 2002.

[12] Motorola, "XMMAS40G10D micromachined accelerometer," Datasheet, Phoenix AZ, available at *www.datasheetarchive.com/XMMAS40G10D-datasheet.html.*

[13] Gaura. Elena, Kraft. M, "Noise Considerations for closed loop digital accelerometers," **in** *Proc. 5rd Conf. Modeling and Simulation of Microsystems*, pp. 154-157, Puerto Rico, 2002.

[14] Chi-Tsong. Chen, *Linear System Theory and Design, 3rd edition*, OXFORD UNIVERSITY PRESS, 1999.

[15] Dan. Simon, *Optimal State Estimation*, WILEY INTERSCIENCE, 2006.

[16] Kemin Zhou, John Doyle, *Essentials of Robust Control*, Prentice-Hall 1998.

[17] G. Pang, Hugh. Liu, "Evaluation of a Low-cost MEMS Accelerometer for Distance Measurement," *Journal of Intelligent and Robotic Systems*, vol. 30, pp 249-265, Netherlands, 2001.

[18] L. Zimmermann, J. Ebersohl, etc, "Airbag application: a Microsystem including a silicon capacitive accelerometer, CMOS switched capacitor electronics and true self-test capability," *Sensors and Actuators*, A 46-47, pp.190-195, 1995.

[19] Chirayu. Shah, "Sensorless Control of Stepper Motor Using Kalman Filter," M. S. Thesis, Department of Electrical and Computer Engineering, Cleveland State University, 2004.

[20] KyuYeon. Park, ChongW. Lee, HyunS. Jang, "Capacitive type surface-micromachined silicon accelerometer with stiffness tuning capability," *Sensors and Actuators*, vol. 73, pp 109–116, South Korea, 1999.

[21] L A. Rocha, E. Cretu, R F. Wolffenbuttel, “Measuring and Interpreting the Mechanical-Thermal Noise Spectrum in MEMS,” *Journal of Micromechanics and Microengineering*, vol. 15, pp. 30-38, 2005.